

## **General Disclaimer**

### **One or more of the Following Statements may affect this Document**

- This document has been reproduced from the best copy furnished by the organizational source. It is being released in the interest of making available as much information as possible.
- This document may contain data, which exceeds the sheet parameters. It was furnished in this condition by the organizational source and is the best copy available.
- This document may contain tone-on-tone or color graphs, charts and/or pictures, which have been reproduced in black and white.
- This document is paginated as submitted by the original source.
- Portions of this document are not fully legible due to the historical nature of some of the material. However, it is the best reproduction available from the original submission.

NG-R-21-002-066

THE EFFECT OF ADIABATIC FOCUSING UPON  
CHARGED PARTICLE PROPAGATION IN  
RANDOM MAGNETIC FIELDS

James A. Earl

Technical Report No. 75-088

July 1975

(NASA-CR-145473) THE EFFECT OF ADIABATIC  
FOCUSING UPON CHARGED PARTICLE PROPAGATION  
IN RANDOM MAGNETIC FIELDS (Maryland Univ.)  
76 p HC \$4.75

N76-10976

CSCL 03B

Unclas  
39429

G3/93



UNIVERSITY OF MARYLAND  
DEPARTMENT OF PHYSICS AND ASTRONOMY  
COLLEGE PARK, MARYLAND

THE EFFECT OF ADIABATIC FOCUSING UPON CHARGED PARTICLE  
PROPAGATION IN RANDOM MAGNETIC FIELDS

James A. Earl

Department of Physics and Astronomy, University of Maryland, College Park

Received 1975 July 24

ABSTRACT

The charged particles considered in this paper are scattered by random fields while they propagate along the diverging lines of force of a spatially inhomogeneous guiding field. Their longitudinal transport is described in terms of the eigenfunctions of a Sturm-Liouville operator which incorporates the effect of adiabatic focusing along with that of scattering. The relaxation times and characteristic velocities, which appear in this matrix formulation of the transport problem, are graphed and tabulated. The particle density that results from a localized impulsive injection is evaluated as a function of space and time for two different regimes. In the first regime, where focusing is relatively weak, a diffusive mode of propagation is dominant, but coherent modes are also present, and they become prominent as the intensity of focusing increases. In the second regime, where focusing is strong, diffusion does not occur, and the propagation is purely coherent. This supercoherent mode corresponds exactly to the so-called scatter-free propagation of kilovolt solar flare electrons. Moreover, diffusive propagation in the first regime offers an explanation of several poorly understood aspects of solar cosmic-ray events. On a larger scale, focused transport provides an interpretation of many observed characteristics of extragalactic radio sources.

Subject headings: cosmic rays: general - hydromagnetics

## I. INTRODUCTION

The diffusion equation underlies much existing work on solar and galactic cosmic-rays. However, if particle propagation takes place along a diverging guiding field under the influence of adiabatic focusing, the diffusive idealization is valid only if the mean free path for scattering in random fields is small compared to both the scale length for spatial variations of the density and the scale length for spatial variations of the guiding field. This paper describes the deviations from diffusive behavior that occur when neither of these conditions is satisfied. This formulation of transport theory is mathematically similar to the approach that I took in three previous papers (Earl 1973, Paper I, 1974a, Paper II and 1974b, Paper III). Consequently, these papers and the equations therein will be designated below by their roman numerals. Most of these references are to Paper II which analyzed a coherent mode which is qualitatively similar to the supercoherent mode that occurs when adiabatic focusing is sufficiently intense. The systematic effect of focusing considered here is completely different from the stochastic effect considered by Goldstein, Klimas and Sandri (1975), which arises from small scale divergences of the random field.

In §II, the transport problem is formulated in terms of eigenfunctions of an operator which incorporates both scattering by random fields and focusing by a spatially inhomogeneous guiding field. The behavior of these eigenfunctions is described in §III. Focused diffusion, a transitional mode which spans the gap between the purely diffusive transport that occurs when focusing is weak and the purely coherent transport that occurs when focusing is strong, is discussed in §IV. The supercoherent mode is introduced in §V. Thus, the theory developed in these sections not only identifies and describes a novel mode of particle propagation but also establishes its relationship to diffusion.

The existence of pronounced coherent effects opens up many possibilities for the interpretation of astrophysical phenomena. These possibilities are explored in an interplanetary context in §VI where the so-called scatter-free propagation of solar flare electrons is explained and where several poorly understood aspects of solar cosmic-ray events are interpreted. In §VII, the structure of extragalactic radio sources is explained in terms of focused transport. Here, the transport phenomena introduced in this paper give rise not only to the twin lobes of radio emission, which are a basic feature of these sources, but also to many other details of their morphology.

## II. MATRIX FORMULATION OF TRANSPORT THEORY

The particle distribution function  $f(\mu, z, t)$  evolves according to the equation

$$\frac{\partial f}{\partial t} + \mu V \frac{\partial f}{\partial z} = \frac{1}{2} \frac{\partial}{\partial \mu} \phi \frac{\partial f}{\partial \mu} - \frac{V}{2L} (1 - \mu^2) \frac{\partial f}{\partial \mu} \quad (1)$$

in which the effect of adiabatic focusing is represented by the second term on the right hand side (Roelof 1969), which involves the scale length  $L$  for spatial variations of the guiding field,

$$\frac{1}{L} = - \frac{1}{B} \frac{\partial B}{\partial z} \quad (2)$$

In equation (1),  $z$  is distance parallel to the mean field,  $\mu$  is the cosine of the pitch angle,  $V$  is particle velocity, and  $t$  is time. The Fokker-Planck coefficient for pitch angle scattering will be described by

$$\phi(\mu) = A |\mu|^{q-1} (1 - \mu^2) \quad (3)$$

in which  $q$  is the spectral index of the power law that gives the mean square amplitude of field fluctuations at wave number  $k$  within an interval  $dk$ ,  $Q_{xx} (k_0/k)^q dk$ , in terms of the spectral density  $Q_{xx}$  at a reference wave number  $k_0$ . Here, the parameter  $A$ ,

$$A = 2\pi \frac{V}{R^2} Q_{xx} (k_0 r_L)^q \quad (4)$$

can be expressed in terms of the particle rigidity  $R$ , velocity  $V$ , and Larmor radius  $r_L$  and the spectral parameters  $Q_{xx}$ ,  $q$ , and  $k_0$  (Jokipii 1966). Although the validity of the quasilinear approach that underlies equation (4) has been questioned, this simple relationship is invoked here for purposes of illustration with the understanding that the

numerical values of certain parameters, which are expressed below not only as functions of  $q$  and  $A$  but also in general terms, may have to be revised when a consensus is reached on the correct treatment of pitch angle scattering. Such a revision would not affect the qualitative validity of the conclusions reached here.

The assumption that  $L$  is constant, which will be adopted throughout this paper, greatly simplifies the analysis that follows, but as long as  $L$  does not change much within one scattering length, it does not significantly limit the applicability of the results. This assumption implies that the guiding field decreases exponentially, which means that its lines of force diverge from one another as  $z$  increases. Because of this divergence, the lateral area over which particles are spread increases with  $z$ , for particle transport perpendicular to the field lines proceeds relatively slowly. Consequently, the normalization that corresponds to a fixed total number of particles is

$$N_0 = \frac{1}{2} \int_{-1}^{+1} \int_{-\infty}^{+\infty} e^{z/L} f(u, z, t) du dz = \int_{-\infty}^{+\infty} e^{z/L} F_0(z, t) dz \quad (5)$$

in which the exponential factor takes into account this variation in the area over which the isotropic density  $F_0$  is spread.

When equation (1) is integrated over  $u$  from  $-1$  to  $+1$ , the scattering term contributes nothing because  $\phi$  vanishes at both limits, while the focusing term can be integrated by parts to yield

$$\frac{\partial F_0}{\partial t} = - \left[ \frac{\partial}{\partial z} + \frac{1}{L} \right] S \quad (6)$$

where  $S$  is the streaming flux defined by

$$S = (v/2) \int_{-1}^{+1} u f du . \quad (7)$$

Because the expression in square brackets is the divergence operator (Roelof 1969), equation (6) expresses an important and familiar equality between the temporal rate of change of the density  $F_0$  and the negative divergence of the flux.

Papers I, II, and III invoked expansions of  $f$  in terms of eigenfunctions of the scattering operator which appears as the first term on the right hand side of equation (1). To describe the effects of focusing, this paper invokes eigenfunctions of a very similar operator which also includes the focusing term. Thus, the focusing eigenfunctions  $Q_K\{\mu\}$ , which are defined in the same spirit as the scattering eigenfunctions  $R_K\{\mu\}$ , satisfy the following equation:

$$\frac{d}{d\mu} \phi \frac{dQ_K}{d\mu} - \frac{V}{L} (1 - \mu^2) \frac{dQ_K}{d\mu} + \frac{2}{\sigma_K} Q_K = 0 \quad (8)$$

where the eigenvalue  $(2/\sigma_K)$ , which replaces the scattering eigenvalue  $(2/\tau_K)$ , describes the temporal decay of an anisotropy proportional to  $Q_K$ . Equation (8) can also be written in the form

$$\frac{d}{d\mu} e^{-G} \phi \frac{dQ_K}{d\mu} + \frac{2}{\sigma_K} e^{-G} Q_K = 0 \quad (9)$$

where the function  $G\{\mu\}$  which appears in the exponential,

$$G\{\mu\} = \frac{V}{L} \int_0^\mu \frac{1-v^2}{\phi\{v\}} dv = \frac{V}{AL} \frac{\mu^{2-q}}{(2-q)}, \quad (10)$$

is the same as the one defined by equation (III-32) except for a scale factor  $(1/L)$ . The important parameter  $(V/AL)$ , which is the ratio of the scattering length  $(V/A)$  to the scale  $L$  of guiding field variations, characterizes the intensity of focusing. The following boundary condition, which is to be imposed at  $\mu = +1$  and at  $\mu = -1$ , completes the specification of the eigenfunctions and ensures that they are well behaved:

$$\phi \frac{dQ_K}{d\mu} = 0 . \quad (11)$$

In the limit  $L \rightarrow \infty$ ,  $Q_K = R_K$ , but, in contrast to the situation discussed previously, where even numbered  $R_K$  were even functions of  $\mu$  and odd numbered  $R_K$  were odd functions, the  $Q_K$  have no special symmetry when  $L$  is finite. In its usual sense as a description of spatial symmetry, the word parity is obviously inappropriate here. Nevertheless, this word will be used below in its mathematical sense to designate whether the indices of eigenfunctions are odd or even.

Because equation (9) has the form prescribed by Sturm-Liouville theory, the functions  $Q_K$  form an orthogonal set in terms of which the distribution function can be expressed as a series expansion

$$f(\mu, z, t) = \sum f_K(z, t) d_K Q_K(\mu) \quad (12)$$

where the factor  $d_K$  defined by

$$\frac{1}{d_K} = \left( \int_{-1}^{+1} e^{-G} Q_K^2 d\mu \right)^{\frac{1}{2}} \quad (13)$$

converts  $Q_K$  into a normalized eigenfunction and where the coefficients  $f_K$  are given by

$$f_K = d_K \int_{-1}^{+1} e^{-G} Q_K f d\mu . \quad (14)$$

In equations (13) and (14), which typify the integrals that occur when orthogonality is invoked,  $\exp\{-G\}$  is a weighting function which emphasizes the contribution from the region  $\mu < 0$  where the odd function  $G$  is negative. This asymmetry, which becomes very pronounced when  $(V/AL)$  is large, makes focused transport qualitatively different from rectilinear transport.

When equation (12) is substituted in equation (1), orthogonality implies that the coefficients  $f_K$  are described by a set of differential equations the first four of which are

$$\frac{\partial f_0}{\partial t} + U_{00} \frac{\partial f_0}{\partial z} = -U_{01} \frac{\partial f_1}{\partial z} - U_{02} \frac{\partial f_2}{\partial z} - U_{03} \frac{\partial f_3}{\partial z} \quad (15)$$

$$\frac{\partial f_1}{\partial t} + \frac{f_1}{\sigma_1} + U_{11} \frac{\partial f_1}{\partial z} = -U_{01} \frac{\partial f_0}{\partial z} - U_{12} \frac{\partial f_2}{\partial z} - U_{13} \frac{\partial f_3}{\partial z} \quad (16)$$

$$\frac{\partial f_2}{\partial t} + \frac{f_2}{\sigma_2} + U_{22} \frac{\partial f_2}{\partial z} = -U_{02} \frac{\partial f_0}{\partial z} - U_{12} \frac{\partial f_1}{\partial z} - U_{23} \frac{\partial f_3}{\partial z} \quad (17)$$

$$\frac{\partial f_3}{\partial t} + \frac{f_3}{\sigma_3} + U_{33} \frac{\partial f_3}{\partial z} = -U_{03} \frac{\partial f_0}{\partial z} - U_{13} \frac{\partial f_1}{\partial z} - U_{23} \frac{\partial f_2}{\partial z} \quad (18)$$

where the characteristic velocities,

$$U_{JK} = U_{KJ} = V d_{JK} \int_{-1}^{+1} \mu e^{-G} Q_J Q_K d\mu, \quad (19)$$

play the role of matrix elements that couple the temporal evolution of the coefficients to their gradients. This matrix formulation of transport theory is analogous to that derived previously (see eq. [II-10] - [II-13]), but it differs in that each coefficient is coupled to its own gradient through the diagonal velocity elements  $U_{KK}$  which appear on the left hand sides of equations (15) - (18). Moreover, the source terms on the right hand sides of these equations embody coupling between coefficients of similar parity that did not appear in previous papers where the characteristic velocities corresponding to  $U_{02}$  and  $U_{13}$  were zero. However, in the limit  $L \rightarrow \infty$ , the matrix elements that couple coefficients of opposite parity,  $U_{01}$ ,  $U_{03}$ ,  $U_{12}$ , and  $U_{23}$ , reduce to the same characteristic velocities,  $V_{01}$ ,  $V_{03}$ ,  $V_{12}$ , and  $V_{23}$ , that appeared in Paper II.

The first eigenfunction,  $Q_0 = \text{constant}$ , is an isotropic component which satisfies equation (8) provided that the relaxation time  $\sigma_0$  is infinite. Because all of the higher order eigenfunctions are orthogonal to  $Q_0$ , they must satisfy

$$\int_{-1}^{+1} e^{-G} Q_K d\mu = 0, \quad (20)$$

but this condition does not imply that the isotropic density associated with the higher-order eigenfunctions is zero, for this weighted integral is not the same as the unweighted average that gives the density. More specifically, the density is given by

$$F_0 = \frac{1}{2} \int_{-1}^{+1} f d\mu = \sum \langle Q_K \rangle f_K \quad (21)$$

where

$$\langle Q_K \rangle = \frac{1}{2} d_K \int_{-1}^{+1} Q_K(\mu) d\mu \quad (22)$$

is the average density associated with  $Q_K$ . Similarly, according to equation (7), the flux is

$$S = \sum V_K f_K$$

where the velocity  $V_K$  defined by

$$V_K = \frac{1}{2} V d_K \int_{-1}^{+1} \mu Q_K(\mu) d\mu \quad (24)$$

characterizes the flux associated with  $Q_K$ . Because the expressions for density and flux involve all components, the situation is different from that in unfocused transport where the density is identical to the isotropic component and where, consequently, the lowest-order matrix equation is also the flux equation. Instead, the derivative  $(\partial F_0 / \partial t)$  that appears in the flux equation (eq. [6]) must be calculated by

summing the quantities  $\langle Q_K \rangle (\partial f_K / \partial t)$  predicted by the matrix equations (eqs. [15] - [18]). In the resulting expression,

$$\begin{aligned} \frac{\partial F_0}{\partial t} = & - [\langle Q_0 \rangle u_{00} + \langle Q_1 \rangle u_{01} + \langle Q_2 \rangle u_{02} + \dots] \frac{\partial f_0}{\partial z} \\ & - [\langle Q_0 \rangle u_{01} + \langle Q_1 \rangle u_{11} + \langle Q_2 \rangle u_{12} + \dots] \frac{\partial f_1}{\partial z} - \frac{\langle Q_1 \rangle f_1}{\sigma_1} \\ & - [\langle Q_0 \rangle u_{02} + \langle Q_1 \rangle u_{12} + \langle Q_2 \rangle u_{22} + \dots] \frac{\partial f_2}{\partial z} - \frac{\langle Q_2 \rangle f_2}{\sigma_2} \\ & - \dots \end{aligned} \quad (25)$$

the sums within square brackets reduce to

$$[\langle Q_0 \rangle u_{0K} + \langle Q_1 \rangle u_{1K} + \dots] = \frac{1}{2} V d_K \int_{-1}^{+1} \mu Q_K d\mu \equiv V_K \quad (26)$$

which is an identity that follows from equation (24) when the integrand  $\mu Q_K$  is expanded in an eigenfunction series with the aid of equations (14) and (19). A second identity, which relates  $V_K$  to the relaxation time  $\sigma_K$ ,

$$\frac{\langle Q_K \rangle}{\sigma_K} = \frac{V_K}{L} \quad (27)$$

follows from

$$\begin{aligned} V \int_{-1}^{+1} \mu Q_K d\mu &= -\frac{V}{2} \int_{-1}^{+1} (1 - \mu^2) \frac{dQ_K}{d\mu} d\mu = \\ &= -\frac{L}{\sigma_K} \int_{-1}^{+1} G' e^G dv \int_{-1}^v e^{-G} Q_K d\mu = \frac{L}{\sigma_K} \int_{-1}^{+1} Q_K d\mu \end{aligned} \quad (28)$$

in which the first equality results from an integration by parts, the second from the following substitutions (see eqs. [9] and [10]):

$$\phi \frac{dQ_K}{d\mu} = \frac{2e^G}{\sigma_K} \int_{-1}^{\mu} e^{-G} Q_K d\mu$$

$$\frac{dG}{d\mu} = G' = \frac{V}{L} \frac{1 - \mu^2}{\phi(\mu)},$$

and the third from a further integration by parts. When these identities are invoked in equation (25), it reduces to the flux equation, for the gradient terms sum to  $(\partial S/\partial z)$  while the  $(\langle Q_K \rangle f_K/\sigma_K)$  terms sum to  $(S/L)$ . If some of the matrix equations are left out of this summation, the flux equation is not satisfied. Consequently, when the integral specified by equation (5) is performed upon the solutions of a truncated set of matrix equations, the resulting total number of particles changes with time. Although this deviation from proper normalization is disconcerting, it has minor significance as long as the real temporal evolution is rapid compared to the relatively slow decay artificially introduced by truncation.

### III. FOCUSING EIGENFUNCTIONS AND EIGENVALUES

Focusing eigenfunctions are analogous to the familiar orthogonal functions that occur in classical and quantum physics. In particular, when  $q = 1$  and  $(V/AL) = 0$ , they reduce to Legendre polynomials. But it is only in such exceptional cases that analytical methods yield closed expressions for eigenvalues and characteristic velocities. In general, these parameters must be evaluated numerically. There is no need to present here the lengthy details of this evaluation, for the final results are sufficient to specify completely the matrix formulation of transport theory. Nevertheless, it is appropriate to outline briefly the method that gave these results. It was basically the iterative method of Stodola and Vianello (Hildebrand 1949, Chap. 5) supplemented by the procedures described by Boulidis and Ruggiero (1944) for determining higher order eigenfunctions. For each value of  $q$ , scattering eigenfunctions for  $(V/AL) = 0$  were calculated by iteration starting with the approximate eigenfunctions derived in Paper II-§II as the initial trial functions. Then  $(V/AL)$  was incremented in small steps. At each step, new eigenfunctions were calculated using the eigenfunctions from the previous step as initial trial functions. The main objective of this section is to present graphs that show how these eigenfunctions and the parameters derived from them as specified in §II depend upon  $q$  and  $A$ .

For weak focusing, a workable alternative to numerical methods is to treat the focusing term as a perturbation whose effect can be approximated with the aid of standard quantum mechanical perturbation formulae. In a preliminary version of this paper, perturbations of the approximate scattering eigenfunctions given in Paper II were evaluated

with the aid of second-order theory. Although most of the results in §IV were first obtained through this procedure, it was eventually abandoned, because an intractable divergence of the perturbation expansions made it impossible to analyze the strong focusing limit discussed in §V. But, in the course of this exercise, several useful relationships were discovered. Although the perturbation approach will not be pursued, it does confirm the fundamental validity of these identities, which appear here as numerical coincidences.

In the discussion that follows, three specific values of the spectral index are given special emphasis. The first,  $q = 1.0$ , corresponds to the isotropic scattering considered in classical transport theory. Thus, the results obtained for this index illustrate the effect of focusing upon classical rectilinear transport. The second index,  $q = 1.5$ , approximates that observed for magnetic fluctuations in space. Thus, the predictions obtained for this index apply to the interplanetary propagation of solar and galactic cosmic-rays. The third value,  $q = 1.9$ , corresponds to very anisotropic scattering. In this situation, the eigenfunctions can be evaluated numerically, but they are qualitatively similar to those for  $q > 2$ , where the evaluation is complicated by the divergent behavior of the function  $G$  defined by equation (10). Thus, the results obtained for this index indicate how focusing affects the coherent regime discussed in Paper II.

The effect of focusing, for  $q = 1.5$ , is illustrated in Figure 1 where the focusing eigenfunctions for  $(V/AL) = 1$  are compared with the scattering eigenfunctions. The latter functions, at the left, exhibit two qualities which also characterize Legendre polynomials. (See Abramo-

witz and Stegun, 1964, Fig. 22.8.) First, the number of zeros between  $\mu = -1$  and  $\mu = +1$  is equal to the index. Second,  $R_1$  and  $R_3$ , whose indices are odd numbers, are odd functions of  $\mu$ , while  $R_0$  and  $R_2$ , whose indices are even, are even functions. Because the first of these features is a consequence of general theorems ( Courant and Hilbert, 1953, Ch. 6.), it also appears in the focusing eigenfunctions, at the right, where the zeros are shifted slightly toward smaller values of  $\mu$  but where their number is unchanged. The second symmetry, which is a characteristic of rectilinear transport, is less fundamental. Thus, the focusing eigenfunctions display a prominent asymmetry such that their absolute magnitude is generally larger when  $\mu > 0$  than it is when  $\mu < 0$ . This asymmetry becomes very pronounced for large values of  $(V/AL)$  where all eigenfunctions are small except in the vicinity of  $\mu = +1$  where they are large and positive. Within the scope of this paper, a comparison of observational details with theory is not possible. Nevertheless, it is worth noting here the striking similarity of the  $Q_1$  anisotropy in Figure 1 to the angular distributions reported for solar protons and electrons by Nielsen, Pomerantz and West (1975).

In Figure 2, eigenvalue spectra are plotted as functions of  $(V/AL)$  for the three spectral indices mentioned above. In all cases, the deviation of the eigenvalue  $(2/A\sigma_K)$  from its unperturbed value  $(2/At_K)$  increases quadratically with small values of the parameter  $(V/AL)$  and linearly with large values. For  $q = 1.5$  and  $q = 1.9$ , this linear increase of  $(2/A\sigma_1)$  and  $(2/A\sigma_2)$  is such that these eigenvalues differ by a small and nearly constant separation, but for  $q = 1.0$ , the increase is such that they become equal at  $(V/AL) = 11.5$ . This degeneracy disappears

at  $q = 1.2$ . On the other hand, when focusing is absent, the spectrum for  $q = 1.9$  foreshadows the degenerate behavior that appears when  $q > 2$ , for  $(2/A\sigma_1)$  is nearly equal to zero and  $(2/A\sigma_2)$  is nearly equal to  $(2/A\sigma_3)$ . Because this convergence does not occur when  $(V/AL) > 0$ , it can be inferred that focusing removes the degeneracies, discussed in Paper II, that characterize the coherent regime. This inference was confirmed at  $q = 2.0$  by a detailed analysis which also showed that the dependence of  $(2/A\sigma_1)$  upon  $(V/AL)$  is purely linear. A tendency toward this disappearance of the quadratic regime is evident in Figure 2. Similarly, in the strong focusing limit, the existence of a quadratic regime affects the intercept of the linear relationship but not the slope. Thus, in this limit where  $(V/AL) \rightarrow \infty$ , the eigenvalues vary as  $(2/\sigma) \propto (V/L)$ . They do not depend sensitively upon the parameters  $q$  and  $A$  which describe scattering.

Figure 3 shows how the four velocities that have finite values in the absence of focusing,  $U_{01}$ ,  $U_{03}$ ,  $U_{12}$  and  $U_{23}$ , depend upon  $(V/AL)$ . In all cases, they approach zero in the strong focusing limit. For sufficiently anisotropic scattering, exemplified by the curves for  $q = 1.5$  and  $q = 1.9$  at the right, this approach takes the form of a monotonic decrease with  $(V/AL)$  which sets in at smaller values of this parameter and becomes more precipitous as  $q$  increases. For isotropic scattering, illustrated by the curve for  $q = 1.0$  at the left, the velocities  $U_{01}$  and  $U_{23}$  decrease monotonically, but  $U_{03}$  and  $U_{12}$  go through maxima and minima before decreasing.

The six characteristic velocities that vanish when focusing is absent are shown in Figure 4. For weak isotropic scattering, they exhibit the intricate behavior shown at the left by the curve for  $q = 1$ ,

but as  $(V/AL) \rightarrow \infty$ ,  $U_{00}$ ,  $U_{11}$  and  $U_{33}$  decrease slowly toward large negative values. Similarly,  $U_{13}$  and  $U_{02}$  increase from small negative values toward zero, while  $U_{22}$  becomes large and positive. When the scattering becomes anisotropic, this complicated and unsymmetrical pattern simplifies dramatically as is illustrated at the right by the curves for  $q = 1.5$  and  $1.9$ . Here, the velocities that couple coefficients of odd parity to themselves,  $U_{11}$  and  $U_{33}$ , and to each other,  $U_{13}$ , are positive and relatively large, while the velocities that couple those of even parity to themselves,  $U_{00}$  and  $U_{22}$ , and to each other,  $U_{02}$ , are negative and relatively large. This pattern gives rise to the supercoherent modes discussed in §V. In the strong-focusing limit, the coupling between coefficients of opposite parity, which causes diffusive effects, becomes weak for anisotropic scattering. This absence of coupling has a quantitative reality that cannot be adequately described by the graphical representation in figures 2 and 3. For example, when  $q = 1.5$  and  $(V/AL) = 6$ ,  $U_{23}$ , which is the largest of the velocities that couple unlike parities, is only 6% of  $U_{02}$ , which is the smallest of those that couple like parities. When  $(V/AL) = 10$ , this ratio decreases to 0.1%.

Table 1 gives numerical values of the three eigenvalues and ten characteristic velocities. From these entries, all of the parameters defined below can be calculated.

## IV. FOCUSED DIFFUSION

In the weak focusing regime, which coincides approximately with the quadratic regime of Figure 2, all of the characteristic velocities are large enough to be significant, but the higher-order relaxation times are much smaller than  $\sigma_1$ . Under these circumstances, as was discussed in Paper I, the coefficients  $f_2$  and  $f_3$ , which are approximately proportional to  $\sigma_2$  and  $\sigma_3$ , play a relatively minor role. Consequently, focused diffusion, which is the fundamental mode that occurs here, can be discussed in terms of a truncated set of matrix equations in which the two lowest order coefficients,  $f_0$  and  $f_1$ , are retained in equations (15) and (16), but the small coefficients of higher order eigenfunctions are neglected. These equations, which are

$$\frac{\partial f_0}{\partial t} + U_{00} \frac{\partial f_0}{\partial z} = - U_{01} \frac{\partial f_1}{\partial z} \quad (29)$$

$$\frac{\partial f_1}{\partial t} + \frac{f_1}{\sigma_1} + U_{11} \frac{\partial f_1}{\partial z} = - U_{01} \frac{\partial f_0}{\partial z} \quad (30)$$

involve three velocities,  $U_{00}$ ,  $U_{01}$ , and  $U_{11}$ , and one relaxation time  $\sigma_1$ . In the discussion that follows, they will be solved with the aid of the methods invoked in Paper II. However, it is worth considering first the result of eliminating  $f_1$  from equations (29) and (30)

$$\frac{\partial^2 f_0}{\partial t^2} + \frac{1}{\sigma_1} \frac{\partial f_0}{\partial t} - U_{01}^2 \frac{\partial^2 f_0}{\partial z^2} = - (U_{00} U_{11}) \frac{\partial^2 f_0}{\partial z^2} - (U_{00} + U_{11}) \frac{\partial^2 f_0}{\partial z \partial t} - \frac{U_{00}}{\sigma_1} \frac{\partial f_0}{\partial z} \quad (31)$$

in which the left hand side is the telegrapher's equation (eq. [II-35]).

The terms on the right hand side, which embody the effect of focusing, vanish when  $L \rightarrow \infty$ . Thus, in this limit, the solutions given below reduce to

the well known results discussed in Paper II-§III.

To obtain these solutions, it is appropriate to express both  $f_0$  and  $f_1$  as Fourier integrals over wavenumber  $\kappa$

$$f_0(z,t) = \int_{-\infty}^{+\infty} d\kappa \alpha(\kappa) e^{i\kappa z + i\omega t}, \quad f_1(z,t) = \int_{-\infty}^{+\infty} d\kappa \beta(\kappa) e^{i\kappa z + i\omega t}, \quad (32)$$

in which, by virtue of equations (29) and (30), the amplitudes  $\alpha$  and  $\beta$  must satisfy

$$(\omega + U_{00}\kappa)\alpha + U_{01}\kappa\beta = 0, \quad (33)$$

$$U_{01}\kappa\alpha + (\omega + U_{11}\kappa - i/\sigma_1)\beta = 0. \quad (34)$$

Because these are linear homogeneous equations, the two frequencies for which they have a solution must satisfy a quadratic equation,

$$(\omega + U_{00}\kappa)(\omega + U_{11}\kappa - i/\sigma_1) - U_{01}^2\kappa^2 = 0, \quad (35)$$

which states that the determinant of the coefficients vanishes. These

frequencies,  $\omega_+$  and  $\omega_-$ , which can be written in the form

$$\omega_{\pm} = (i/\sigma_*) + V_c\kappa \pm iV_*[\kappa_1^2 - (\kappa - i\kappa_2)^2]^{\frac{1}{2}} \quad (36)$$

where

$$\sigma_* = 2\sigma_1 \quad (37)$$

$$V_* = [U_{01}^2 + \frac{1}{2}(U_{00} - U_{11})^2]^{\frac{1}{2}}, \quad (38)$$

$$V_c = -\frac{1}{2}(U_{00} + U_{11}), \quad (39)$$

$$\kappa_1 = \frac{U_{01}}{2\sigma_1 V_*}, \quad (40)$$

$$\kappa_2 = \frac{U_{11} - U_{00}}{4\sigma_1 V_*}, \quad (41)$$

correspond to normal modes for which the ratio  $(\beta/\alpha)$  does not change with time.

The general solution can be expressed as a linear combination of these modes that satisfies appropriate initial conditions. Two factors complicate its specification. In the first place, the isotropic density

$$\begin{aligned} F_0 &= \langle Q_0 \rangle f_0 + \langle Q_1 \rangle f_1 \\ &= \int_{-\infty}^{+\infty} dk e^{ikz} [(\langle Q_0 \rangle \alpha_+ + \langle Q_1 \rangle \beta_+) e^{i\omega_+ t} + (\langle Q_0 \rangle \alpha_- + \langle Q_1 \rangle \beta_-) e^{i\omega_- t}] \end{aligned} \quad (42)$$

which is what experiments measure, should be described rather than the individual components  $f_0$  and  $f_1$ . In the second place, the initial anisotropy must be more carefully treated in focused transport, where it has an important effect upon the evolution of the density, than in purely diffusive transport, where it has a minimal effect. The solutions given below describe how the density depends upon space and time after the injection of a localized pulse with a finite initial velocity. In this situation, the injection velocity specifies the initial anisotropy in a physically meaningful way.

The initial conditions that correspond to such an injection at  $t = 0$ ,  $z = 0$ , of a pulse moving in the  $+z$  direction with a velocity  $V_+$  are first

$$F_0\{z,0\} = N_0 \delta\{z\} = \frac{N_0}{2\pi} \int_{-\infty}^{+\infty} dk e^{ikz}, \quad (43)$$

in which  $\delta\{z\}$  is the Dirac delta function, and second

$$F_0\{z,t\} = e^{-z/L} F\{z - V_+ t\}$$

in which the exponential factor is necessary for proper normalization and which is equivalent to

$$\frac{\partial F_0}{\partial t} = -v_+ \left[ \frac{\partial}{\partial z} + \frac{1}{L} \right] F_0 . \quad (44)$$

The linear combination of modes that matches these conditions must satisfy two equations involving the amplitudes  $\alpha_+$ ,  $\alpha_-$ ,  $\beta_+$  and  $\beta_-$ ,

$$[\langle Q_0 \rangle \alpha_+ + \langle Q_1 \rangle \beta_+] + [\langle Q_0 \rangle \alpha_- + \langle Q_1 \rangle \beta_-] = N_0/2\pi , \quad (45)$$

and

$$\begin{aligned} & [\omega_+ + v_+(\kappa - i/L)] [\langle Q_0 \rangle \alpha_+ + \langle Q_1 \rangle \beta_+] \\ & + [\omega_- + v_+(\kappa - i/L)] [\langle Q_0 \rangle \alpha_- + \langle Q_1 \rangle \beta_-] = 0 , \end{aligned} \quad (46)$$

which correspond respectively to the first and second conditions. When the solution of these equations is substituted in equation (42),  $F_0$  is given by

$$F_0 = \frac{N_0}{2\pi} \int_{-\infty}^{+\infty} d\kappa e^{i\kappa z} \frac{[\omega_+ + v_+(\kappa - i/L)] e^{i\omega_- t} - [\omega_- + v_+(\kappa - i/L)] e^{i\omega_+ t}}{\omega_+ - \omega_-} \quad (47)$$

which is similar in form to equation (II-47).

With the aid of equation (36), this expression can be rewritten as

$$\begin{aligned} F_0 = \frac{N_0}{2v_*} \exp\{ - (t/\sigma_*) - \kappa_2(z + v_c t) \} & \left[ \frac{1}{\sigma_*} + v_+(\kappa_2 - \frac{1}{L}) + \right. \\ & \left. + \kappa_2 v_c + \frac{\partial}{\partial t} - (2v_c + v_+) \frac{\partial}{\partial z} \right] P(z, t) , \end{aligned} \quad (48)$$

in which the propagation function  $P$  is defined by

$$\begin{aligned} P(z, t) &= \frac{1}{2\pi i} \int_{-i\infty}^{+i\infty} ds \exp\{-s(z + v_c t)\} \frac{\exp\{V_* t(\kappa_1^2 + s^2)^{1/2}\} - \exp\{-V_* t(\kappa_1^2 + s^2)^{1/2}\}}{(\kappa_1^2 + s^2)^{1/2}} \\ &= I_0\{\kappa_1(V_+ t - z)^{1/2} (z + v_- t)^{1/2}\} , \quad -V_- t < z < +V_+ t, \\ &= 0 , \quad , \quad z < -V_- t ; z > +V_+ t, \end{aligned} \quad (49)$$

where  $s = -i\kappa - \kappa_2$  is the Laplace transform variable invoked by Abramowitz

and Stegun (1964, eq. [29.3.92]). Near the origin, P behaves as a modified Bessel function, but it jumps to zero at two discontinuities, one of which moves in the +z direction with velocity

$$V_+ = V_* - V_c, \quad (50)$$

while the other moves in the -z direction with velocity

$$V_- = V_* + V_c. \quad (51)$$

At the discontinuities, the numerical value of P remains constant at unity. Between them, it grows monotonically with time to form a bell shaped spatial profile whose peak moves in the -z direction with velocity  $V_c$ . Thus, the phenomena predicted by equation (48) are qualitatively similar to those discussed in Paper II-5III. More specifically, the spatial and temporal derivatives of the step discontinuities in P give rise to  $\delta$  functions which represent two localized pulses moving in opposite directions. Initially, these coherent disturbances contain all of the particles injected, but as trajectories are scattered, the number of particles in an extended wake, which is spread continuously between the pulses, grows larger. This wake, which arises from the continuous portion of P, develops into a moving Gaussian analogous to the familiar diffusive profile.

Because of the artifact mentioned above, equation (47) is not properly normalized to a constant total number of particles. Thus, when the integration specified by equation (5) is performed, the integral over z gives a delta function in  $\kappa$ ,  $\delta\{i/L\}$ , which immediately leads to

$$\int_{-\infty}^{+\infty} e^{z/L} F_0(z,t) dz = N_0 \frac{\omega_+\{i/L\}e^{i\omega_-\{i/L\}t} - \omega_-\{i/L\}e^{i\omega_+\{i/L\}t}}{\omega_+\{i/L\} - \omega_-\{i/L\}}. \quad (52)$$

Because equation (36) specifies that the frequencies  $\omega_+(i/L)$  and  $\omega_-(i/L)$  are both positive imaginary numbers, this expression represents a sum of two exponentials decaying with different time constants. Similar sums arise in the radioactive decay of genetically related nuclides and in the fragmentation of cosmic-rays, but in contrast to these situations where the initial number of secondary particles is zero, the coefficients in equation (52) are such that the initial slope is zero. Consequently, there is a brief period after injection during which the normalization integral is virtually constant. Then, it decays at an exponential rate corresponding to  $\omega_-(i/L)$  which is the smaller frequency. Figure 5 shows how the ratio  $\sigma_1 \omega_-(i/L)$  of this rate to the rate  $1/\sigma_1$ , which characterizes the overall evolution of the distribution function, depends upon  $(V/AL)$ . In all cases, the normalization failure is insignificant in the weak focusing limit where this ratio varies as  $(V/AL)^4$ . In the case of isotropic scattering,  $q = 1$ , the normalization failure becomes intolerable in the strong focusing limit where the ratio approaches unity. In the case of anisotropic scattering, on the other hand, the normalization failure is not very important, for the maximum relative decay rates are only 8% and 5% at  $q = 1.5$  and  $q = 1.9$ , respectively. However, even these small deviations from proper normalization can lead to significant effects at long times after the injection. Thus when  $t \gg 1/\omega_-(i/L)$  and also when the scattering is isotropic and focusing is intense, the solutions given here are not accurate. Under these circumstances, higher-order components, such as  $f_2$  and  $f_3$ , should be taken into account.

The average density  $\langle F_0 \rangle$  is defined as an unweighted integral of  $F_0$  over  $z$ . In this integration of equation (47), the factor  $\exp\{z/L\}$  does

not appear, and the delta function becomes  $\delta\{0\}$  which leads to

$$\langle F_0 \rangle = \int_{-\infty}^{+\infty} F_0(z,t) dz = N_0 - N_0 (v_+ \sigma_1 / L) (1 - e^{-t/\sigma_1}) . \quad (53)$$

The average density is proportional to the number of particles injected, but it also depends upon initial conditions and time. The latter dependences are not surprising, because the local density depends, as a result of guiding field convergence, not only upon the number of particles present but also upon where they are located. For isotropic injection,  $v_+ = 0$ , the average density is the same as if focusing were absent. This average density also occurs just after injection with a finite velocity, but the transient component decays with time constant  $\sigma_1$  to give at equilibrium an enhanced density for  $v_+ < 0$  and a reduced density for  $v_+ > 0$ . An interesting example of this behavior is the case  $v_+ = (L/\sigma_1)$  in which the average density decays to zero.

In Paper II, the density  $f_0$  was expressed as the following weighted sum of two elementary disturbances  $f_0^+$  and  $f_0^-$  associated, respectively, with coherent pulses moving in the  $+z$  and  $-z$  directions:

$$f_0(z,t,v_+) = \frac{1}{2}[1 + (v_+/v_{01})]f_0^+ + \frac{1}{2}[1 - (v_+/v_{01})]f_0^- ,$$

where

$$f_0^+ = N_0 e^{-t/2\tau_1} \left[ \delta(z - v_{01}t) + \frac{I_0 \{ (1/2\tau_1 v_{01}) (v_{01}^2 t^2 - z^2)^{\frac{1}{2}} \}}{4\tau_1 v_{01}} \right. \\ \left. + \frac{(z + v_{01}t)^{\frac{1}{2}} I_1 \{ (1/2\tau_1 v_{01}) (v_{01}^2 t^2 - z^2)^{\frac{1}{2}} \}}{(v_{01}t - z)^{\frac{1}{2}} 4\tau_1 v_{01}} \right] ,$$

$$f_0^- = N_0 e^{-t/2\tau_1} \left[ \delta(z + v_{01}t) + \frac{I_0 \{ (1/2\tau_1 v_{01}) (v_{01}^2 t^2 - z^2)^{\frac{1}{2}} \}}{4\tau_1 v_{01}} \right. \\ \left. + \frac{(v_{01}t - z)^{\frac{1}{2}} I_1 \{ (1/2\tau_1 v_{01}) (v_{01}^2 t^2 - z^2)^{\frac{1}{2}} \}}{(z + v_{01}t)^{\frac{1}{2}} 4\tau_1 v_{01}} \right] , \quad (54)$$

which is equation (II-51) repeated to facilitate comparison. The analogous result obtained from equations (48) and (49) is

$$F_0(z, t, V_+) = \frac{1}{2}[1 + (V_c + V_+)/V_*]F_0^+ + \frac{1}{2}[1 - (V_c + V_+)/V_*]F_0^- ,$$

where

$$F_0^+ = N_0 \exp\{- (t/\sigma_*) - \kappa_2(z + V_c t)\} \left[ \left[ \delta(z - V_+ t) + \frac{1}{2V_*} \left[ \frac{1}{\sigma_*} + V_c \kappa_2 + V_+ \left( \kappa_2 - \frac{1}{L} \right) \right] I_0\{y\} + \frac{\kappa_1}{2} \frac{(z + V_- t)^{\frac{1}{2}}}{(V_+ t - z)^{\frac{1}{2}}} I_1\{y\} \right] \right] ,$$

$$F_0^- = N_0 \exp\{- (t/\sigma_*) - \kappa_2(z + V_c t)\} \left[ \left[ \delta(z + V_- t) + \frac{1}{2V_*} \left[ \frac{1}{\sigma_*} + V_c \kappa_2 + V_+ \left( \kappa_2 - \frac{1}{L} \right) \right] I_0\{y\} + \frac{\kappa_1}{2} \frac{(V_+ t - z)^{\frac{1}{2}}}{(z + V_- t)^{\frac{1}{2}}} I_1\{y\} \right] \right] , \quad (55)$$

and where  $y$  is the argument of the Bessel function that appears in equation (49). The rectilinear transport described by the first of these expressions differs from the focused transport described by the second in the following respects:

(1) The weighting factors  $\frac{1}{2}[1 \pm (V_c + V_+)/V_*]$  are such that the contribution of  $F_0^-$  vanishes when  $V_+ = V_+$  while that of  $F_0^+$  vanishes when  $V_+ = -V_-$ . The corresponding disappearance of  $f_0^+$  and  $f_0^-$  occurs at equal positive and negative velocities,  $V_+ = \pm V_{01}$ . However, in all cases, if the injection velocity coincides with the velocity of either coherent pulse, then the other pulse is absent.

(2) In addition to a temporal dependence similar to that in equation (54), the exponential factor in equation (55) also embodies a spatial dependence such that the pulse moving in the  $-z$  direction is enhanced relative to the one moving in the  $+z$  direction.

(3) In contrast to  $f_0^+$  and  $f_0^-$  which are independent of the injection velocity, the elementary disturbances  $F_0^+$  and  $F_0^-$  depend

explicitly upon  $V_+$  through the factor multiplying the  $I_0$  component of the wake.

(4) In the arguments of the Bessel functions and in the factor multiplying the  $I_1$  component, the parameter  $(1/2\tau_1 V_{01})$  that appears in equation (54) is replaced by  $\kappa_1$  in equation (55).

Because of its complexity, the implications of equation (55) are best discussed, as is done below, in terms of limiting cases for which a simplification occurs. To give perspective on these illustrations, figure 6 shows how the velocities of the coherent pulses depend upon  $(V/AL)$ . When the scattering is anisotropic, as it is at  $q = 1.5$  and  $q = 1.9$ ,  $V_-$  is slightly larger than  $V_+$ , and in the strong focusing limit, both velocities increase slowly with  $(V/AL)$ . However, when  $q = 1$ , the coherent velocities diverge, for  $V_-$  increases as before while  $V_+$  continues to decrease with  $(V/AL)$ . Perturbation theory led to the identity  $\kappa_2 = (1/2L)$ . The approximate validity of this relationship is demonstrated, for  $q = 1.5$  and  $q = 1.9$ , in figure 7 where the product  $2\kappa_2 L$  lies within a few percent of unity over a wide range of  $(V/AL)$ . The dotted curve, which refers to the co-ordinate scale at the right, shows that the relationship is also valid within  $\pm 20\%$  for  $q = 1.0$  provided that  $(V/AL) < 5$ .

The Gaussian limit of equation (54) applies when  $V_{01}t \gg |z|$  and  $t/2\tau_1 \gg 1$ . Under these circumstances, in which the Bessel functions approach their asymptotic form  $\exp\{y\}/(2\pi y)^{1/2}$ , the square root appearing in their arguments can be expanded with the aid of the binomial theorem to yield

$$f_0(z,t) = \frac{F_0 \exp\{-z^2/4Dt\}}{2(\pi Dt)^{1/2}} \quad (56)$$

which is the familiar Green's function for one dimensional diffusion from an impulsive injection at  $t = 0$  localized at  $z = 0$ , and which involves the coefficient of diffusion  $D \approx \tau_1 v_{01}^2$ . (See eq. [II-43] for a more direct derivation of this expression.) Similarly, when  $v_* t \gg |z + v_c t|$  and  $\kappa_1 v_* t \gg 1$ , and if the second terms in the asymptotic expansions of  $I_0$  and  $I_1$  (Abramowitz and Stegun, 1964, eq. [9.7.1]) are also taken into account, equation (55) reduces to

$$F_0 = N_0 C \exp\left\{\frac{t}{\tau_{\#}} + \frac{\tau_+}{t} - \kappa_2 \lambda\right\} \left[ \frac{\exp\left\{-\frac{(z + v_{\#} t - \lambda)^2}{4D_{\#} t}\right\}}{2(\pi D_{\#} t)^{1/2}} \right], \quad (57)$$

where

$$D_{\#} = \frac{v_*}{2\kappa_1} = \frac{\sigma_1 v_*^3}{U_{01}} \quad (58)$$

is an important new parameter that I call the coefficient of focused diffusion, where

$$v_{\#} = v_c + (\kappa_2/\kappa_1)v_* \approx v_c + (D_{\#}/L) \quad (59)$$

is the velocity with which the peak of the bracketed Gaussian moves in the  $-z$  direction, and where

$$\frac{1}{\tau_{\#}} = \frac{(v_* - U_{01})^2}{4\sigma_1 v_* U_{01}} \quad (60)$$

describes an exponential growth that does not occur in the absence of focusing. Similarly, the factor

$$C = \frac{1}{2} \left[ 1 + \frac{v_*^2 + \frac{1}{2}(U_{00}^2 - U_{11}^2) + \frac{1}{2}v_+(U_{11} - U_{00} - 4\sigma_1 v_*^2/L)}{U_{01} v_*} \right] \quad (61)$$

depends upon  $v_+$  and deviates from the value of unity that it has in equation (56).

The length  $\lambda$ , given by

$$\lambda = \frac{\sigma_1 V_* (V_c + V_+)}{C U_{01}} \quad (62)$$

represents a small displacement of the  $z$  co-ordinate which arises because injection occurs, in effect, over the distance covered by the initial pulse before it decays rather than strictly at  $z = 0$ . The time  $\tau_+$ , given by

$$\tau_+ = \frac{\sigma_1 V_*}{4 U_{01}} \left[ 1 - \frac{2}{C} + \left( \frac{V_c + V_+}{C V_*} \right)^2 \right] \quad (63)$$

characterizes a small correction which depends upon the injection velocity but which becomes negligible as  $t$  increases. These two corrections arise from the second terms mentioned above. Although they do have a minor effect upon rectilinear transport, they do not appear in the standard Gaussian approximation where isotropic injection is implicitly assumed. They were taken into account here in an attempt to improve the accuracy of the Gaussian representation, but for many purposes they can be neglected.

Equations (57)-(60) have three implications which mean that focused diffusion is strikingly different from ordinary diffusion. In the first place, the point of maximum density, which occurs at  $z = \lambda - V_{\#} t$  where the argument of the Gaussian function is zero, moves in the  $-z$  direction with velocity  $V_{\#}$ . In ordinary diffusion, the Gaussian remains centered at  $z = \lambda$ . In the second place, the coefficient  $D_{\#}$  is substantially larger than  $D$  whenever  $(V/AL)$  is large. In the third place, the factor  $C \exp\{t/\tau_{\#}\}$  multiplying the Gaussian not only depends upon the injection velocity  $V_+$ , but also increases exponentially with time.

To provide a reference to ordinary diffusion against which these implications can be compared, figure 8a, at the left, shows profiles of density vs  $z$ , for  $q = 1.5$ , at the instant  $t = (10/A) \approx 4\tau_1$  following an injection with  $V_+ = +V_{01}$ . The wake calculated from equation (54), which is rigorously exact and which is shown as a solid line, drops discontinuously to zero at  $z = \pm V_{01}t$ . Because the velocities at injection are collimated in the  $+z$  direction, the wake peaks at a point,  $z \approx V_{01}\tau_1 = \lambda$ , to the right of the point of injection. Following a suggestion made in Paper II, the coherent disturbance (dotted curve) is represented here by a Gaussian whose width  $(D_*t)^{1/2}$  is characterized by a coefficient of dispersion  $D_* = (D/20)$ . Within the region where the density in the wake is finite, the dashed line, which represents the Gaussian predicted by equation (57) for  $L = \infty$ , provides a fairly accurate description of the actual wake. Near the maximum, the two curves are nearly coincident, but the Gaussian is about 25% too low at  $z = +V_{01}t$  where the asymptotic expressions for the Bessel functions are not accurate. For  $|z| > V_{01}t$ , the Gaussian gives a finite density which misrepresents the actual value of zero. Nevertheless, the contribution of this incorrect prediction to the total area under the dashed curve compensates for the underestimated density in the range  $|z| < V_{01}t$  in such a way that the area under the Gaussian is the same as that under the exact profile. Thus, in the case of ordinary diffusion, the Gaussian approximation is correctly normalized. For injection toward the left with  $V_+ = -V_{01}$ , the profile is the mirror image obtained by reflecting around  $z = 0$  the profile for  $V_+ = +V_{01}$ .

In figure 8b, profiles are shown for focused diffusion with  $(V/AL) = 1.0$ ,  $q = 1.5$ ,  $t = (10/A)$  and  $V_+ = +V_+ = 0.549V$ . Because these profiles,

at the center, refer to the same time and to nearly the same positive injection velocity as those for ordinary diffusion, at the left where  $V_+ = V_{01} = 0.563V$ , the qualitative differences that are immediately apparent must be attributed to focusing. Even though the injection is toward the  $+z$  direction, the wake is largest near the discontinuity at  $z = -V_-t$ . Near the other discontinuity at  $z = +V_+t$ , the density in the wake is relatively small. Consequently, the coherent pulse, which is represented as before by a Gaussian plotted as a dotted line, seems insignificant even though it contains 53% of the injected particles. Because the velocity  $V_{\#} = 1.081V$  is greater than  $V_- = 0.631V$ , the Gaussian peak lies far to the left of  $V_-t$ . Consequently, the density predicted by equation (57) (dashed line, for which  $D_{\#} = 1.07(V^2/A) = 1.34D$ ) decreases monotonically with increasing  $z$  from its maximum value at  $-V_-t$ . This decrease does not reproduce the exact prediction of equation (55) (solid line) which exhibits a maximum just to the right of  $-V_-t$ . Nevertheless, the largest difference between solid and dashed curves is only 6%. It is apparent in figure 8b, where the vertical scale is expanded by a factor of 3 over that in figure 8a, that the density in the wake for focused diffusion with positive injection velocities is much smaller than that for ordinary diffusion.

In figure 8c, which refers to the same conditions as figure 8b except that the injection velocity is negative,  $V_+ = -V_-$ , the exact profile (solid line) decreases monotonically from its maximum at  $z = -V_-t$ . The wake, which is plotted on a vertical scale reduced relative to that of figure 8b by a factor of 10 and relative to that of figure 8a by a factor of 3.33, is much larger than the wake associated

with ordinary diffusion or with focused diffusion after injection toward diverging guiding fields. The coherent pulse (dotted line), which is 313 times larger than the one in figure 8b, is a prominent feature of the density profile, but it contains only .12% of the injected particles. The Gaussian approximation (dashed line) peaks well to the left of  $z = -V_-t$ . It approximates the solid profile with a maximum deviation of 22%.

Because the bracketed expression in equation (57) has the form of a normalized Gaussian, the expression multiplying it represents the total area under the approximate profile from  $z = -\infty$  to  $z = +\infty$ . Obviously, from figures 8b and 8c, this area has no straightforward relationship to the area under the exact profile, for most of it lies near the peak in a region where the density actually is zero. Consequently, the expression multiplying the brackets should be regarded as one which gives an accurate approximation and not as a normalization parameter.

The tendency of the Gaussian peak to outrun the discontinuity moving in the  $-z$  direction must disappear when focusing is very weak, for the unfocused Gaussian is stationary. This disappearance is illustrated in figure 6 where the dotted line representing  $V_+$  crosses the solid line representing  $V_-$  at a value of  $(V/AL)$  below which focused diffusion is governed by the extreme weak focusing limit discussed in the next paragraph. Evidently, this value becomes small as  $q \rightarrow 2$ .

To interpret solar particle events, many authors have assumed that interplanetary propagation is governed by the diffusion equation for

spherical geometry. In the present context, this equation corresponds to the result of substituting into equation (6) a first-order approximation to the flux,  $S = -D(\partial F_0/\partial z)$ , (see Paper III) to yield a diffusion equation

$$\frac{\partial F_0}{\partial t} - \frac{D}{L} \frac{\partial F_0}{\partial z} = D \frac{\partial^2 F_0}{\partial z^2} . \quad (64)$$

With the aid of the transformation

$$w = z + (D/L)t ,$$

equation (64) can be put in a form,

$$\frac{\partial F_0}{\partial t} = D \frac{\partial^2 F_0}{\partial w^2} , \quad (65)$$

whose solution,

$$F_0 = N_0 \frac{\exp\{-w^2/4Dt\}}{2(\pi Dt)^{1/2}} = N_0 \frac{\exp\{-[z + (D/L)t]^2/4Dt\}}{2(\pi Dt)^{1/2}} , \quad (66)$$

is a Gaussian similar to the one in equation (57) except that  $D$  appears in the place of  $D_{\#}$ . Equation (66) does not take into account the quantitative difference between these coefficients, it does not include the exponential growth that occurs when focusing is intense, and it does not describe either the prominent coherent pulses or the pronounced dependence upon propagation velocity that characterize focused diffusion. Because these considerations also apply to the diffusion equation for spherical geometry, existing work on interplanetary diffusion should be re-examined from a point of view which correctly incorporates the effect of focusing.

The limit  $\kappa_1 V_{\star} t \rightarrow 0$  is a simple case that illustrates the transition from focused diffusion to supercoherent propagation but that does not

depend upon the detailed properties of Bessel functions. In this special case, where  $I_0 = 1$  and  $I_1 = 0$ , equation (55) reduces to

$$F_0(z,t) = N_0 \exp\{- (t/\sigma_*) - \kappa_2(z + V_c t)\} \left[ \left[ \frac{1}{2}[1 + (V_c + V_+)/V_*] \delta(z - V_+ t) + \frac{1}{2}[1 - (V_c + V_+)/V_*] \delta(z + V_- t) + \frac{1}{2V_*} \left[ \frac{1}{\sigma_*} - \frac{(V_+ - V_c)}{2L} \right] \right] \right] \quad (67)$$

in which the identity  $\kappa_2 = (1/2L)$  has been invoked. Here, the coherent  $\delta$  functions are weighted as before, and the wake spread between them depends upon  $z$  and  $t$  only through the exponential multiplying the brackets. In the diffusive regime, the Gaussian form reached by the wake is virtually independent of conditions at injection, but in the relatively strongly focused regime exemplified by equation (67), the wake depends critically upon  $V_+$ . In particular, if  $V_+ = V_c$  and  $L = \frac{1}{2} \sigma_* (V_* - 2V_c)$ , the wake is completely absent, and there is only one coherent pulse. It moves toward regions of reduced guiding field while its amplitude decreases as  $\exp\{- (z/L)\}$ . Because the exponential factor appearing in equation (5) compensates for this decrease in density, the total number of particles in the pulse is constant. On the other hand, if  $V_+ = -V_-$ , there is one coherent pulse moving with constant amplitude into stronger guiding fields. There is also a substantial wake whose density decreases exponentially with distance away from the pulse. In this situation, according to equation (5), the number of particles in the pulse decreases exponentially with time, but this decrease is accompanied by a growth of the number in the wake such that the total remains constant.

As was discussed in Paper II-§III, the first of these examples embodies the most pronounced alignment in the  $+z$  direction of particle

velocities at injection that can be adequately treated in a description which invokes only the two components  $f_0$  and  $f_1$ . In this situation, the wake is insignificant and nearly all of the injected particles remain in a coherent pulse whose amplitude decreases rapidly as a result of the geometrical divergence of field lines but very slowly as a result of scattering. Qualitatively, this stability of the number of particles within a bunch whose velocities are collimated along the guiding field occurs because the rate at which they are realigned by adiabatic focusing exceeds the rate at which they are scattered. In the second example, on the other hand, the same effect works in the opposite direction, for focusing aids scattering by rapidly removing particles from a bunch whose velocities are aligned in the  $-z$  direction. In spite of this rapid reduction in the number of particles, the density within the bunch remains stable, because particles moving in this direction converge together laterally along with the guiding lines of force. Because particles removed from the pulses constitute the source of the wake, the above considerations also explain why the wake associated with an injection toward stronger guiding fields is more pronounced than the one associated with an injection toward weaker fields.

## V. THE SUPERCOHERENT MODE

The discussion in §IV outlined the changes which occur as the intensity of focusing is increased while other conditions are unchanged. In the weak focusing limit described by equation (66), where the scattering length ( $V/A$ ) is much smaller than  $L$ , the Gaussian profile of ordinary diffusion drifts slowly into stronger guiding fields. In focused diffusion described by equation (57), where  $(V/A) \approx L$ , the drift velocity exceeds the particle velocity, the diffusive wake, which is no longer a bell shaped Gaussian, is dependent upon conditions at injection, and the coherent disturbances are very prominent. In the strongly focused regime described by equation (67), where  $(V/A) \gtrsim L$ , coherent effects dominate and the wake is insignificant. In the supercoherent mode to be discussed in this section, which occurs when  $(V/A) \gg L$ , the tendency of focusing to enhance coherent transport and to suppress diffusive transport reaches a limit in which the wake is completely absent and particle propagation is coherent. The word supercoherent is appropriate here because transport phenomena in this regime are analogous to those in the superfluid and superconductive states. Unlike these states, the supercoherent mode does not appear at a discontinuous phase transition. However, the supercoherent transition does occur very abruptly with the disappearance of the velocities in figures 3b and 3c which embody the coupling between coefficients of opposite parity that leads to diffusive effects.

Because the three negative velocities in figures 4b and 4c display almost the same pattern as the three positive velocities, it might be expected that a second supercoherent mode would propagate in the direction opposite to the one that actually does propagate in the  $+z$  direction. In fact, the second mode decays rapidly and leaves its particles in an extended wake. The

reason for this decay can be seen in equation (25) where the expression within square brackets that multiplies  $(\partial f_0/\partial z)$  must vanish according to equation (26). But the terms proportional to  $U_{01}$  and  $U_{03}$  are small when  $(V/AL)$  is large, while those proportional to  $U_{00}$  and  $U_{02}$  are large and negative. Consequently, because the truncated form of this expression takes on negative values instead of the required value  $V_0 = 0$ , the flux equation is not even approximately satisfied when  $f_0$  and  $f_2$  are finite. Thus, a mode that propagates coherently in the  $-z$  direction can be constructed as a linear combination of  $Q_0$  and  $Q_2$ , but it can not be properly normalized. In this situation, which involves strongly focused disturbances that move in the  $-z$  direction, a perturbation approach analogous to that employed in Paper III is more appropriate than the method of eigenfunctions. Such an approach cannot be pursued here, but its qualitative effect can be judged in Figure 8c where dispersive effects would mix together the triangular wake and the coherent pulse to give a broad disturbance propagating quasi-coherently in the  $-z$  direction with an effective velocity of  $U_{00}$ . I call this the pseudodiffusive mode.

Only a few of the positive terms that appear inside the bracketed expressions multiplying  $(\partial f_1/\partial z)$  and  $(\partial f_2/\partial z)$  in equation (25) are needed to approximate  $V_1$  and  $V_3$ . Consequently, an accurately normalized supercoherent mode can be constructed as a linear combination of  $Q_1$  and  $Q_3$ . Because these eigenfunctions are not coupled to  $Q_0$  and  $Q_2$ , only the two odd transport equations are required to describe this mode. This simplification is similar to the one that appeared in Paper II-§IV where the purely coherent modes that occur when  $q > 2$  were discussed in terms of two transport equations. However, these modes, which arise because pitch angle scattering is very weak near  $\mu = 0$ , are physically different from the supercoherent mode,

which occurs because the tendency of focusing to align particle velocities overcomes the tendency of scattering to make them isotropic.

The equations which describe the supercoherent mode were obtained from equations (16) and (18) by neglecting the small gradient terms in  $U_{01}$ ,  $U_{03}$ ,  $U_{12}$  and  $U_{23}$  while retaining the large ones in  $U_{13}$ ,  $U_{11}$  and  $U_{33}$ . They are,

$$\frac{\partial f_1}{\partial t} + U_{11} \frac{\partial f_1}{\partial z} + \frac{f_1}{\sigma_1} = - U_{13} \frac{\partial f_3}{\partial z} \quad (68)$$

$$\frac{\partial f_3}{\partial t} + U_{33} \frac{\partial f_3}{\partial z} + \frac{f_3}{\sigma_3} = - U_{13} \frac{\partial f_1}{\partial z} . \quad (69)$$

Because their form is very similar to that of equations (29) and (30), there is no need to derive in detail the solutions discussed below, for each step corresponds exactly to a step taken in §IV to derive solutions for focused diffusion. Thus, the frequencies  $\omega_+$  and  $\omega_-$  can be obtained by substituting into equation (36) the following expressions:

$$\sigma_* = \frac{2\sigma_1 \sigma_3}{\sigma_1 + \sigma_3} , \quad (70)$$

$$v_* = [U_{13}^2 + \frac{1}{2}(U_{11} - U_{13})^2]^{\frac{1}{2}} , \quad (71)$$

$$v_c = - \frac{1}{2}(U_{11} + U_{13}) , \quad (72)$$

$$\kappa_1 = \frac{U_{13}}{2v_*^2} \left( \frac{1}{\sigma_3} - \frac{1}{\sigma_1} \right) , \quad (73)$$

$$\kappa_2 = \frac{U_{33} - U_{11}}{4v_*^2} \left( \frac{1}{\sigma_3} - \frac{1}{\sigma_1} \right) . \quad (74)$$

Because the parameters that specify  $\omega_+$  and  $\omega_-$  are the same as those that appear in equation (55), these redefinitions determine completely the exact solutions that apply in the supercoherent regime.

If these frequencies are substituted in equation (52), it predicts truly minuscule deviations from proper normalization. In contrast, the frequencies that apply to the mode that propagates in the  $-z$  direction, which follow from two transport equations obtained from equations (15) and (17),

$$\frac{\partial f_0}{\partial t} + U_{00} \frac{\partial f_0}{\partial z} = - U_{02} \frac{\partial f_2}{\partial z} , \quad (75)$$

$$\frac{\partial f_2}{\partial t} + U_{22} \frac{\partial f_2}{\partial z} + \frac{f_2}{\sigma_2} = - U_{02} \frac{\partial f_0}{\partial z} , \quad (76)$$

lead to an extremely rapid decay of the normalization integral. This analysis establishes the positive-velocity supercoherent mode as a unique and fundamental feature of strongly focused transport.

In spite of the mathematical identity embodied in equations (70)-(74), supercoherent propagation is different from focused diffusion. In the latter regime, where  $V_c$  is small and  $V_*$  is large, the bell shaped profile of the propagation function drifts slowly in the  $-z$  direction while the discontinuities move rapidly in opposite directions. This configuration leads to the diffusive evolution of a wake spread between two coherent pulses. In the former region, where  $V_c$  is large and  $V_*$  is small, both discontinuities of the propagation function move in the  $+z$  direction, and the bell shaped profile spread between them also moves in the same direction with an intermediate velocity. This configuration leads to the unidirectional propagation of localized disturbances. The velocity  $V_a$  of the leading discontinuity ahead of which there are no particles is given by

$$V_a = \frac{1}{2}(U_{11} + U_{13}) + V_* , \quad (77)$$

while the velocity  $V_b$  of the trailing discontinuity behind which there are no particles is given by

$$V_b = \frac{1}{2}(U_{11} + U_{13}) - V_* . \quad (78)$$

If the injection velocity  $V_+$  is positive and if it lies between  $V_a$  and  $V_b$ , the density profile is given by equation (55). This rigorous solution includes a coherent disturbance associated with each discontinuity, but

these higher-order pulses, which are analogous to those discussed in Paper II-§IV, rapidly become insignificant compared to the continuous profile. The breadth of this profile can be determined from figure 9 where the velocities of its boundaries,  $V_a$  and  $V_b$ , are plotted against  $(V/AL)$  for  $q = 1.5$  and  $q = 1.9$ . If  $V_+ > V_a$ , equation (55) does not hold, because eigenfunctions above  $Q_3$  must be included in a proper description of the strong anisotropies implied by this initial condition. However, these anisotropies decay rapidly to leave a situation similar to the one that follows the injection of a pulse with velocity  $V_a$ . Because the same consideration also applies to the strongly anisotropic injection of solar particles, profiles calculated with  $V_+ = V_a$  are most appropriate for comparison with observations. If  $V_+ < V_b$ , the supercoherent disturbance, which is very similar to the one that follows injection with  $V_+ = V_b$ , is accompanied by a broad pseudodiffusive wake moving in the  $-z$  direction. The proper description of this disturbance also involves eigenfunctions above  $Q_3$ , but negative or small positive injection velocities do not correspond to solar injection. Thus, for virtually all plausible initial conditions, the supercoherent profile can be accurately described by substituting the parameters defined by equations (70)-(74) in equation (55).

The Gaussian limit of this solution, which applies when  $V_* t \gg |z - V_c t|$ , is

$$F_0 = N_0 C \exp\left\{-\frac{t}{\tau_s} - \kappa_2 \lambda\right\} \left[ \frac{\exp\left\{-\frac{(z - V_s t - \lambda)^2}{4D_s t}\right\}}{2(\pi D_s t)^{1/2}} \right], \quad (79)$$

where

$$D_s = \frac{V_*}{2\kappa_1} = \frac{\sigma_1 \sigma_3}{\sigma_1 - \sigma_3} \frac{V_*^3}{U_{13}} \quad (80)$$

is the coefficient of supercoherent dispersion which plays much the same role as the coefficient of dispersion  $D_*$  defined in Paper II-§IV, where

$$V_{\xi} = -V_c - \frac{\kappa_2}{\kappa_1} V_* = \frac{1}{2} \left(1 + \frac{V_*}{U_{13}}\right) U_{11} + \frac{1}{2} \left(1 - \frac{V_*}{U_{13}}\right) U_{33} \quad (81)$$

is the supercoherent velocity with which the peak of the Gaussian moves in the  $+z$  direction, and where

$$\frac{1}{\tau_{\xi}} = \frac{1}{\sigma_1} - \left(\frac{1}{\sigma_3} - \frac{1}{\sigma_1}\right) \frac{(V_* - U_{13})^2}{4V_* U_{13}} \quad (82)$$

describes an exponential decay of the amplitude. The factor

$$C = \frac{1}{2} \left[ 1 + \frac{\left(\frac{\sigma_1 + \sigma_3}{\sigma_1 - \sigma_3}\right) V_*^2 + \frac{1}{2}(U_{11}^2 - U_{33}^2) - \frac{1}{2}V_* \left(U_{11} - U_{33} + \frac{4\sigma_1 \sigma_3}{\sigma_1 - \sigma_3} \frac{V_*^2}{L}\right)}{V_* U_{13}} \right] \quad (83)$$

embodies the dependence of the supercoherent Gaussian upon injection velocity.

The offset is given by

$$\lambda = \frac{\sigma_3 \sigma_1}{\sigma_1 - \sigma_3} \frac{V_* (V_+ + V_c)}{U_{13} C} \quad (84)$$

The correction characterized by  $\tau_+$  is negligible.

In figure 9a, the dotted line which represents  $V_{\xi}$  for  $q = 1.5$  almost coincides with the dashed line which represents  $V_+$ . In figure 9b, where  $q = 1.9$ , this coincidence is nearly exact, but, for clarity, only the dotted line is shown. This means that the supercoherent Gaussian moves with virtually the same velocity as the coherent delta function of focused diffusion. In Paper II-§IV, the coherent Gaussians, which had the same velocity as the coherent delta functions, embodied an improved representation of coherent disturbances in which dispersion was included. Similarly, it appears here that the consideration of higher-order eigenfunctions leads to an improved representation which embodies the dispersive evolution of the supercoherent

disturbance. To carry this line of reasoning one step further, if the supercoherent pulse is equivalent to the delta function in equation (67), then the wake predicted there should give a reasonable estimate of the small diffusive wake that remains in the supercoherent regime.

These points are illustrated in figure 10 where a supercoherent pulse for  $q = 1.5$ ,  $(V/AL) = 5$ ,  $V_+ = V_a = .8V$  and  $t = (2/A)$  is shown by a solid line, which represents the exact solution, and by a dotted line, which represents the Gaussian approximation. Associated with this pulse is a wake predicted by equation (67) which is also shown as a solid line. Because  $\kappa_2$  is negative,  $\exp\{-\kappa_2 z\}$  increases with  $z$ . Because of this weighting, the supercoherent velocity  $V_5$  is only slightly less than the velocity  $V_a$  of the leading discontinuity, and the profile drops to zero just in front of its peak. Consequently, the Gaussian width  $(D_5 t)^{1/2}$  overestimates the actual width. However, this complication does not occur when  $t \rightarrow \infty$ . The same weighting effect, which puts the Gaussian peak in a region where the asymptotic representation of the Bessel functions is not accurate, underlies the  $\sim 15\%$  difference by which the exact and approximate peaks are separated in figure 10.

In figure 10, the dashed wake and Gaussian pulse are those of figure 8b with their horizontal scale transformed in such a way that this profile for focused diffusion corresponds to the same time and to the same value of  $L$  as the supercoherent profile, but to scattering 5 times more intense. This change in  $A$ , which goes across the supercoherent transition, leads to a dramatic increase in the magnitude of the wake relative to that of the pulse. However, the dotted supercoherent Gaussian has about the same shape as the dashed coherent one. More quantitatively, the effect of increasing  $(V/AL)$  from 1 to 5 is to reduce the coefficient of dispersion from a virtually unfocused value

$D_* = .0405 (v^2/A)$  to the supercoherent value  $D_g = .0123 (v^2/A)$ . This reduction by a factor of 3.3 is slightly overcompensated by the factor of 5 decrease in A, but the supercoherent Gaussian is not perceptibly wider because the width, at a given time, has a weak square-root dependence upon the coefficient of dispersion.

The Gaussian supercoherent pulse embodies an equilibrium pitch angle distribution in which the opposing effects of scattering and focusing balance. Because of the collimation produced by focusing, stochastic variations in the pitch angle of an individual particle average to give a net velocity which is finite and approximately equal to that of the other particles in the bunch. Statistical fluctuations in this averaging of random velocities give rise to dispersion. This section has put this physical picture on a rigorous basis.

## VI. INTERPLANETARY PROPAGATION OF ENERGETIC PARTICLES

Twenty years ago, Meyer, Parker and Simpson (1956) concluded that diffusion could explain the temporal profile of solar cosmic-ray intensity on 23 February 1956. Subsequent investigations have confirmed the basically diffusive nature of particle propagation in interplanetary space, but they have also uncovered many effects that can not be understood in terms of pure diffusion. The objective of this section is to show that several of these unexplained features arise as natural consequences of adiabatic focusing in the spiral interplanetary field. Because the present theory takes into account neither perpendicular diffusion nor convection, it would be premature to attempt a quantitative comparison of observed and predicted solar event profiles. Instead, the discussion that follows gives a qualitative interpretation of prompt events in which these relatively slow processes play a minor role compared to rapid propagation along field lines that trace out a reasonably direct connection between the Earth and a flare on the western limb of the Sun. Focusing must have important effects in cosmic-ray modulation, but this steady state phenomenon, in which convection plays a crucial role, also lies beyond the scope of the present discussion.

One of the most striking and least understood aspects of interplanetary physics is the "scatter-free" propagation of kilovolt flare electrons in which an impulsive burst of particles, usually followed by a slowly decaying tail, arrives at Earth with an average velocity parallel to the field of  $\approx 0.8V$  (Lin 1974). From observations of Type III radio noise generated by this bunch of electrons, Lin, Evans, and Fainberg (1973) have demonstrated that it travels  $\approx 1.2$  AU along a spiral field line. Although this phenomenon corresponds to the coherent mode discussed in Paper II, there are two discrepancies which make untenable an interpretation based upon this agreement.

In the first place, the predicted velocity is closer to 50% of the particle velocity than it is to 80%. In the second place, developments in scattering theory subsequent to Paper II indicate that scattering near  $\mu = 0$  is not weak enough to allow the purely coherent mode to persist (Jones, Kaiser and Birmingham 1973, Volk 1973, Owens 1974). These discrepancies do not apply to the supercoherent mode, for it occurs even in the presence of scattering at  $\mu = 0$ , and its velocity is close to the observed one. Thus, we can interpret "scatter-free" events as supercoherent bunches which propagate with very little dispersion in the strongly diverging fields near the sun. In this situation, the parameter  $(V/AL)$  is not constant, for the scale length of the interplanetary field is approximately  $(r/2)$  where  $r$  is the distance to the sun. Moreover, the radial dependence of  $(V/A)$  undoubtedly leads to additional variations of the focusing parameter. If  $(V/AL)$  lies above the supercoherent transition, these variations merely cause the supercoherent velocity to change without affecting the basic nature of the mode. This decrease in parallel velocity corresponds exactly to the "deceleration" of the Type III exciter reported by Evans, Fainberg and Stone (1973). However, it occurs because the pitch angle distribution of particles with a given speed becomes broader as focusing decreases, and not because the speed of an individual particle changes. Thus, the observed transit time, which represents an average over a gradual decrease in velocity, corresponds to a velocity larger than the local one. However, this enhancement should be small, because regions where the velocity is slow are more heavily weighted than are those where it is fast. Most supercoherent events involve electrons, but they can also involve protons. An example is the event on 24 March 1966 (McCracken, Rao and Bukata 1967).

Within the same framework, the properties of two other types of solar burst, reviewed by Kundu (1965), can be understood. The U-type bursts, in

which an ascending frequency branch appears after the descending branch of a Type III burst, are interpreted in terms of closed magnetic lines along which the electron bunch returns toward the sun after moving up from the flare site. The "shortness" of the ascending branch compared to the descending one can be explained in terms of the greater dispersion of a bunch moving pseudodiffusively down into converging lines relative to that of a bunch moving supercoherently upward. The V-type bursts, in which a Type III burst is followed by a brief period of broad-band continuum radiation, can be explained as synchrotron radiation from a nearly isotropic cloud of electrons which forms after the bunch passes through the supercoherent transition. This phenomenon is very similar to those discussed below at greater length.

The chief objection to this interpretation is that the values of  $(V/AL)$  calculated for electrons from observations of interplanetary field fluctuations lie below the supercoherent transition. Thus, in the example discussed in Paper II and presented there as figure 6, where 38 KeV electrons were scattered by fluctuations for which  $P_{\text{XX}} = 6.3 \times 10^{-4} \gamma^2 \text{ Hz}^{-1}$  at  $f_0 = 0.5 \text{ Hz}$  and for which  $q = 1.9$ , the focusing parameter is  $(2V/Ar) = 0.022$  which is well below the value  $(V/AL) \approx 0.5$  required, in figure 3c, for supercoherent propagation. Within the framework of current theories which predict that pitch angle scattering increases with decreasing rigidity, this objection can not be overcome. However, there are compelling intuitive reasons to expect a regime where low rigidity particles follow adiabatically the stochastic wandering of magnetic lines of force with very little scattering relative to the local field direction. The correspondence between the "scatter-free" and supercoherent effects can be regarded as empirical proof of the existence of such a regime where scattering decreases with decreasing rigidity as it merges

into the Alfvénic idealization. Consequently, more theoretical effort should be devoted to exploring the low rigidity limit of pitch angle scattering. Less effort should be devoted to analyzing the detailed dependence of  $\varphi$  upon  $\mu$ , for most of the special significance of weak scattering near  $\mu = 0$  disappears in the present context where focusing moves particles rapidly through this region.

There is a localized region in which the nature of interplanetary propagation changes from supercoherent to diffusive, for the focusing parameter must eventually pass through the supercoherent transition by virtue of its inverse dependence upon  $r$ . In this situation, shown schematically in figure 11, solar particles propagate supercoherently to a fairly abrupt transition (wiggly line) beyond which focused diffusion occurs. In effect, the injection of particles into this region of focused diffusion is highly anisotropic and occurs far from the sun. Thus, because  $V_{\perp} = V_{\parallel} \approx V_{+}$ , the density profile can be described by the function  $F_0^{+}$  given by equation (55) with the origin,  $z = 0$  and  $t = 0$ , chosen to be the place and time at which the supercoherent pulse hits the transition.

A well known prediction of the telegrapher's equation is that, within 2 mean free paths of an impulsive injection, the temporal profile has an abrupt onset followed by a monotonic decay. At larger distances, the profile exhibits a relatively gradual increase from onset to a broad maximum which is followed by a monotonic decrease. Similarly, there is a certain distance from the point of injection within which the maximum density predicted by  $F_0^{+}(z, t)$  occurs at onset and beyond which it occurs after onset. This distance  $z_0$  is given by the positive root of the following quadratic equation:

$$z_0^2 - \left[ \frac{2V_{+}}{(\kappa_1 V_{*})^2} \left( \frac{1}{\sigma_{*}} + \kappa_2 V_{*} \right) \right] z_0 - \frac{4V_{+} V_{*}}{(\kappa_1 V_{*})^2} \left[ \left( \frac{1}{\sigma_{*}} + \kappa_2 V_{*} \right) \left( \frac{1}{\sigma_{*}} + \kappa_2 V_{*} \right) - \frac{V_{-} V_{*} \kappa_1^2}{2} \right] = 0 \quad (85)$$

Because its coefficients are complicated, the implications of this equation are best illustrated by quoting the numerical result  $z_0 = 35.8 (V/A)$  obtained for  $q = 1.5$  and  $(V/AL) = 1$ , which is the case illustrated in figure 8. This distance is 6.3 times larger than 2 mean free paths. Thus, a basic effect of focusing is to enlarge the spatial region within which temporal profiles have abrupt onsets.

The region of focused diffusion can be divided by the dashed line in figure 11, which is located at a distance  $z_0$  beyond the supercoherent transition, into two zones in which flare profiles are qualitatively different. The location of Earth relative to the wiggly and dashed dividing lines in figure 11 depends upon the intensity of interplanetary magnetic fluctuations and upon the velocity and rigidity of the particles being observed. Consequently, the nature of observed flare profiles is expected to show considerable variability from day to day, and, at a given time, it may not be the same for all particle species.

In the zone between the dashed and wiggly lines, dispersive effects broaden the coherent pulse and smear out the discontinuous onset of the wake. Consequently, the temporal profile exhibits a fairly abrupt onset whose duration corresponds to the width of the coherent Gaussian. Then, the intensity decays monotonically from its maximum. Many authors have assumed that the interplanetary diffusion coefficient is the one which appears in the diffusive Gaussian that best fits the profile observed during a given event. But, if this procedure is applied to an abrupt-onset event, the coefficient of dispersion is obtained instead of the coefficient of diffusion. (See Paper II, eq. [94].) This misidentification explains why the coefficient of diffusion seems to be paradoxically small when the overall behavior of the profile corresponds to large mean free paths.

Abrupt-onset flare profiles are very commonly observed not only for the low-energy solar protons and electrons recorded by satellite monitors but also for the high energy nuclei sensed by ground level neutron monitors. Their high probability of occurrence is inconsistent with a purely diffusive picture, because the 2 mean free path zone where they are expected is narrow and lies close to the sun. Because focusing widens this zone and moves the point of injection outward toward Earth, the frequent occurrence of abrupt-onset profiles is a natural feature of the configuration shown in figure 11. To describe in detail the strong initial anisotropies of such events (McCracken 1962, McCracken, Rao and Bukata 1967), it is necessary to evaluate the individual components  $f_0$  and  $f_1$  whose separate behavior differs from that of the linear combination specified by equation (42). This calculation can not be undertaken here, but the enhancement of coherent effects caused by focusing means that anisotropies persist for much longer times than they would in the absence of focusing. On many occasions, the initial anisotropy disappears suddenly about an hour after onset. This phenomenon can be understood from figure 11 as the arrival of a disturbance propagating pseudodiffusively back toward the sun from distant regions of weak focusing where scattering finally succeeds in making the distribution function isotropic.

Beyond the dashed line where maximum intensity occurs after onset, flare profiles resemble those of classical diffusion. If a diffusive Gaussian is blindly fitted to one of these profiles, which are described by equation (57), the best fit occurs, not for the coefficient of ordinary diffusion  $D$ , but instead for the coefficient of focused diffusion  $D_{\#}$ . Because  $D_{\#} > D$ , this misidentification can lead to an overestimate of  $D$ . Moreover, in determining the distance to be invoked in the fitting procedure, both the distance to the supercoherent transition and the offset  $\lambda$  should be subtracted

from the Sun to Earth distance. If these corrections are not subtracted, then  $D_{\#}$  is underestimated.

In the late stages of many flare events, the decay takes on an exponential character which differs from the temporal power law predicted by diffusion but which can be explained by postulating a free-escape boundary far from the Sun (Meyer, Parker and Simpson 1956). Such an exponential decay appears as an inherent characteristic of focused diffusion. Its relaxation time  $\tau_*$ , derived from equation (57), is given by

$$\frac{1}{\tau_*} = \frac{v_{\#}^2}{4D_{\#}} - \frac{1}{\tau_{\#}} \quad (86)$$

This time decreases from its infinite unfocused value to approach  $\tau_* \approx 2\sigma_1$  in the strong focusing limit. Because typically observed relaxation times of many hours are much greater than any plausible value of  $\sigma_1$ , the rate of exponential decay must be controlled by weakly focused diffusion in the outer solar system. An accurate description of this regime would take into account the radial variation of the focusing parameter. This can not be done here, but it seems reasonable to expect that a region of uniform density would be set up in the inner solar system through the rapid equalization of density inhomogeneities by coherent effects. Farther out, gradients would develop in a region of weakly focused diffusion through which particles escape at a rate leading to a slow exponential decay.

The Jovian electron bursts recorded on Pioneer 10 result from the inward propagation of low rigidity particles along interplanetary fields (Chenette, et al. 1974, Teegarden, et al. 1974, Smith, et al. 1975). The supercoherent mode does not apply here, but quasi-coherent propagation into converging fields is predicted by equation (57), for relatively weak focusing, and by the pseudodiffusive idealization, for strong focusing. The brief duration and

10 hr modulation of the Jovian bursts can be explained in terms of these modes, but they are difficult to reconcile with pure diffusion. Outside Jupiter, electrons might propagate supercoherently. Here, the intensity of Jovian bursts would decay more rapidly with distance than it does inside, but their temporal fine structure would be better preserved. Observations of these effects could confirm the asymmetrical nature of focused transport.

Several poorly understood interplanetary phenomena correspond to predicted features of focused transport. However, the current status of pitch angle scattering theory at low rigidities does not allow these features to be quantitatively related to the observed intensity of interplanetary magnetic fluctuations. In particular, a weak scattering regime at low rigidities is indicated not only by supercoherent electron events but also by the findings of Bryant, et al. (1965) in which profiles for proton events were dependent upon the distance travelled  $Vt$  but were independent of rigidity. Such behavior can occur only if  $A$  is a linear function of  $V$  alone, which means that  $(V/AL)$  is independent of both velocity and rigidity. Thus, the observations suggest that a broad region of rigidity-independent scattering lies between the low-rigidity regime, where scattering at a given velocity increases with rigidity, and the high-rigidity regime, where it decreases. The transport theory developed in this paper sidesteps these ambiguities and goes directly to the macroscopic description of density profiles in space and time. These profiles depend ultimately upon only three parameters,  $q$  which characterizes the anisotropy of scattering,  $A$  which characterizes the intensity of scattering, and  $L$  which characterizes the intensity of focusing. Until an improved description of pitch angle scattering comes forth, attempts to relate observed profiles to these parameters may be worthwhile.

## VII. THE STRUCTURE OF EXTRAGALACTIC RADIO SOURCES

Double radio sources, between which there is usually found an optical galaxy, are among the largest and most energetic phenomena of astrophysics. In spite of the detailed knowledge of their structure (Mackay 1971, Fomalont 1969) made available by recent advances in interferometry (Ryle 1975), there is still no generally accepted explanation of these remarkable objects. The interpretation put forth in this section, which adopts a widely held view that the radiating electrons gain their energy within the central galaxy, describes the symmetrical transport of these electrons to great distances from this source and the subsequent evolution of the clouds they form there, but it does not attempt to describe their acceleration. This interpretation rests on the assumption that a large scale magnetic field, which threads through the galaxy, extends far into intergalactic space to form a diverging guiding field along which focused transport occurs. Here, the basic morphology of the double sources arises, in much the same way as in interplanetary propagation, when two bunches of electrons move rapidly out in opposite directions to supercoherent transitions where they form relatively long lasting clouds which constitute the actual radio sources. On the time scale implied by the large separation of the clouds from the central source, the Compton-synchrotron mechanism of energy loss plays an important role which will be mentioned below but which cannot be treated in detail.

The chief objection to this interpretation is that the strong anisotropy of the supercoherent mode might be rapidly attenuated by the collective effects reviewed by Wentzel (1974). However, the conventional view, that these wave effects limit streaming velocities to the Alfvén velocity, applies to steady state conditions. In the absence of reliable knowledge of the intergalactic medium and in view of the slow growth of waves, there is no reason to

believe that scattering could be significantly enhanced during the brief period in which a supercoherent pulse sweeps over a given volume of the medium. In any case, as was documented above, the supercoherent mode can persist in the presence of scattering, including that generated by the particles themselves through collective effects. The interplanetary analogy may be relevant here, for Jovian bursts do persist while generating waves (Smith et al. 1975).

Underlying the striking symmetry of double sources is the symmetry of the guiding field, which arises because Maxwell's equations guarantee that as many lines of force diverge out from a local condensation as converge into it. For example, if intergalactic currents are absent, the field would take on a dipolar character, and, if the central galaxy is surrounded by an expanding medium, the field would develop a radial pattern analogous to that of the interplanetary field. Within these bilateral configurations, electrons propagate and radiate in similar magnetic environments on opposite sides of the source. No matter how the electrons are accelerated, scattering within the central galaxy, which makes them isotropic there, ensures that the two bunches contain equal numbers of electrons. When these bunches hit the supercoherent transitions, particles are rapidly scattered into two clouds. Because these clouds contain equal numbers of isotropically distributed electrons and because their diffusive evolution is slight during the time required for light to travel between them, the two lobes of the radio source appear to have nearly the same luminosity regardless of the angle between their axis and the line of sight. The axis is perpendicular to the  $E$  vector of the polarized emission from the clouds. These predicted symmetries are the same as those observed by Macdonald, Kenderine and Neville (1968), who found that the intensity ratios of double sources in the 3C catalog are strongly clustered near unity and that the polarization are strongly

clustered around the direction perpendicular to the axis. However, Mitton (1972) subsequently found that the latter correlation is less pronounced than it had seemed.

Within this picture, minor deviations from symmetry, which appear in many sources, are possible. For example, large scale shearing motions of the intergalactic medium could displace the supercoherent transitions, which define the two lobes, in different directions along the field line through the central source. This apparent longitudinal displacement of the galaxy from the center of the axis joining the lobes could be accompanied by a lateral displacement perpendicular to the axis and by unequal emission from the lobes. Similar distortions could arise from the uniform motion of a rotating galaxy through the intergalactic medium. Another class of deviations from the canonical pattern, which obviously fits into the picture given here, involves emission from the central galaxy.

The spatial profile of synchrotron emissivity, which underlies observed maps of radio intensity, is not the same as the profile of electron density  $F_0$ , for it also depends upon  $B$ . More specifically, the emissivity is given by

$$\epsilon \propto F_0 B^{\frac{1}{2}(\gamma+1)} \nu^{-\frac{1}{2}(\gamma-1)} \approx F_0 B^{1.8} \nu^{-0.8}, \quad (87)$$

where  $\gamma$  is the electron spectral index and where the second equality gives the dependence expected for a typical radio spectral index of 0.8. In the present context, where the theory does not consider perpendicular transport and where existing maps do not always resolve structure perpendicular to the axis, the most appropriate quantity for comparison with observations is the axial profile of power emitted per unit distance parallel to the field. From the emissivity given above and from the relationship  $n_0 \propto (F_0/B)$ , it follows that this quantity is given by

$$(dP/dz) \propto n_0 B^{\frac{1}{2}(\gamma+1)} \nu^{-\frac{1}{2}(\gamma-1)} \propto F_0 B^{\frac{1}{2}(\gamma-1)} \nu^{-\frac{1}{2}(\gamma-1)} \approx F_0 B^{0.8} \nu^{-0.8} \quad (88)$$

where  $n_0$  is the number of particles per unit distance. In the theory discussed above, where  $B$  depends exponentially upon  $z$ , this equation leads to a weighting

$$(dP/dz) = F_0 \exp\{-\frac{1}{2}(\gamma-1)(z/L)\} \approx F_0 \exp\{-0.8 z/L\} \quad (89)$$

which displaces the radio profile toward the galaxy relative to the density profile. Because of this weighting, most of the radio emission comes from a tiny fraction of the electrons which are nearest the galaxy in relatively strong fields. Moreover, in focused diffusion, the Gaussian peak of the radio profile moves toward stronger fields with a velocity given by

$$V_{\parallel} + (\gamma - 1) (D_{\parallel}/L) \approx \gamma V_{\parallel} \quad (90)$$

Thus, if a series of discrete explosions occurs in the central galaxy, clouds from earlier events drift inward where they appear as weak secondary lobes lying on the axis between the intense lobes from later events. The following double sources with well marked lobes each resolved into a close pair have been reported by Macdonald et. al. (1968): 3C33.1, 3C46, 3C61.1, 3C184.1, and 3C234. These authors also report that, in all these cases, the innermost members are weaker than the outermost. If the explosions occur frequently or if the acceleration is continuous, electrons drifting inward form a continuous bridge between the lobes. Clearcut examples of this behavior are 3C46, 3C274.1, 3C284, 3C430 and 3C452, but more or less continuous emission along the axis is seen in many extragalactic sources. Because the Compton/synchrotron mechanism has more time to act on the electrons in these inner components, their radio spectrum is expected to be steeper than that of the outer lobes. This prediction is in accord with the finding of Macdonald et al. (1968) that the emission from between the main components has a steeper spectrum than the source as a whole.

Radio trails (Wellington, Miley and van der Laan 1973, Miley 1973) are believed to delineate magnetic fields dragged out behind as the central galaxy

moves through a stationary medium. In this magnetospheric configuration (Jaffe and Perola 1973), the velocity of the galaxy may exceed the velocity, defined by equation (90), with which the radio Gaussian drifts forward. Consequently, electron clouds from successive explosions are strung out in a trail behind the primary lobes which form, as before, at supercoherent transitions moving with the galaxy. This interpretation predicts that the radio emission from the tail decreases in intensity systematically with distance from the galaxy while its spectral slope increases. These are the effects found by Miley (1973) in 3C129 and NGC 1265.

Except for the effects interpreted above in terms of ageing and except for the flat spectra of central components, which can be similarly interpreted, the structure of radio sources is not strongly dependent upon frequency (Macdonald et al. 1968, Mackay 1969). This indication that the electron spectral index is uniform means that intergalactic propagation is not strongly dependent upon rigidity. The same conclusion was reached above in regard to interplanetary propagation.

The time required for electron bunches to reach the supercoherent transitions is smaller than that required for the clouds to dissipate. Consequently, the probability of observing a double source in its supercoherent phase is small. Nevertheless, among the many sources that have been studied, it is reasonable to expect that a few are currently in this phase. Such sources would appear as two relatively compact radio lobes moving apart with a velocity slightly less than twice the speed of light. This superluminal velocity of recession is only a little smaller than the velocity found in 3C279 and is the same as that found in 3C273 by Cohen, et al. (1971, see also Whitney, et al. 1971.) Because projection effects lead to an overestimate of the velocity of recession when the axis is not perpendicular to the observer's line of sight, the predicted velocity seems to be in good agree-

ment with those observed in these two quasars.

Compton/synchrotron energy loss during the supercoherent phase sets an upper limit on the size of radio sources. More specifically, the maximum distance  $z_{\max}$  in Kpc at which an electron can arrive with energy  $E$  in GeV is

$$z_{\max} = \frac{.94 \times 10^5}{[W + .0369 \langle B^2 \rangle] E} = \frac{2.1 \times 10^5 (B/\nu)^{3/2}}{W + .0369 \langle B^2 \rangle}, \quad (91)$$

where  $W$  is the photon energy density in  $\text{eV cm}^{-3}$  and  $\langle B^2 \rangle$  is the mean square magnetic field in microgauss ( $\mu\text{G}$ ) averaged over the pitch angle distribution and over the distance travelled by the electron at  $V \approx c$ . The expression following the second equality, whose form is convenient for the analysis of radio data, refers to electrons whose maximum radio emission in a field  $B$  in  $\mu\text{G}$  occurs at frequency  $\nu$  in MHz. If this formula is applied to the radio galaxies observed at  $\nu = 5000$  MHz by Branson et al. (1971) and by Pooley and Henbest (1974), who invoked equipartition to deduce magnetic fields that can be used to approximate  $\langle B^2 \rangle$ , the calculated values of  $z_{\max}$  lie comfortably above the observed semi-major axes by factors of 4 to 10. Similarly, in the extreme case of 3C236, which was studied at  $\nu = 612$  MHz by Willis, Strom and Wilson (1974), where  $B \approx 0.6$  microgauss and where the electron lifetime is set by the microwave background ( $W \approx 0.38 \text{ eV cm}^{-3}$ ) rather than by the synchrotron effect,  $z_{\max} = 16.7$  Mpc, which is somewhat larger than the distance of 2.8 Mpc between the outer lobes of this giant object and the central galaxy. In these examples, energy loss may be significant during the evolution of the clouds, but it is insignificant during the supercoherent phase.

In contrast, for the compact outer lobes of Cygnus A (Hargrave and Ryle 1974), where  $B \approx 290 \mu\text{G}$  and  $\nu = 5000$  MHz,  $z_{\max} = 16.3$  Kpc, which is substantially smaller than the 100 Kpc separation of these components

from the central galaxy. On the basis of arguments similar to those underlying this estimate, these authors reached an equivalent conclusion that the synchrotron lifetime of the electrons in these lobes is less than the time required for light to reach them for the central galaxy.

Several considerations soften the impact of this conclusion. To obtain more accurate values of  $z_{\max}$  than the crude estimates obtained above by substituting in equation (61) the square of the equipartition field, a proper evaluation of  $\langle B^2 \rangle$  should take into account not only the collimated angular distribution of the supercoherent mode, but also the decrease of  $B$  with distance from the central galaxy. It is possible that the reduction in  $\langle B^2 \rangle$  arising from the first of these effects significantly outweighs the enhancement arising from the second. Of greater significance is the possibility that the electron energy density is actually larger than the magnetic energy density, for the transient evolution of electron bunches and clouds can be controlled by fields weaker than the minimum field required for steady state confinement. For the supercoherent phase, this possibility seems especially plausible not only because the lateral pressure, which tends to disrupt the guiding field, is much smaller for a collimated bunch of particles than for an isotropic cloud but also because it is exerted, at a given point, for a shorter period of time. Thus, it seems appropriate to assume that the compact components are emitted by electrons that have just formed superdense clouds after propagating supercoherently across Cygnus A in a field of 120  $\mu\text{G}$  corresponding to equipartition within the extended components. In this situation,  $z_{\max} = 61.2$  Kpc, which is slightly smaller than the actual separation of 100 Kpc, but which could probably be made consistent by invoking a more accurate value of  $\langle B^2 \rangle$  and by taking into account the possibility that equipartition does not apply to the extended components. These arguments show that energy loss significantly affects the propagation

of electrons in Cygnus A and suggests that the pressure exerted by particles may affect the large-scale configuration of the magnetic field. If a substantial flux of nuclei accompanies the pure flux of electrons assumed above, the latter suggestion becomes conclusive. Thus, outward particle pressure, which straightens the lines of force, may underlie the well known tendency for the structure of powerful sources like Cygnus A to be simpler and more regular than that of weaker sources whose field configurations are more easily influenced by motions of the intergalactic medium.

The model of extragalactic radio sources developed here is similar to previous interpretations, reviewed by Longair, Ryle and Scheuer (1973), which assume that relativistic particles carry energy from the central galaxy to the radio lobes. Unlike these interpretations, which invoke local acceleration within the lobes, the radio waves are emitted here by the same electrons that transport the energy. Fundamental characteristics of this transport, which takes place in the same magnetic fields that are required to explain the synchrotron emission, give rise to the basic morphology of radio sources. Specifically, the emission is confined to an axis because electrons propagate parallel to the magnetic field more readily than perpendicular to it. Symmetrical lobes appear on this axis because electrons are deposited at the supercoherent transitions far from the central galaxy where they propagate diffusively. The slow drift velocities which characterize this propagation explain the secondary structure between the main lobes and establish a relationship between double sources and radio trail galaxies. The supercoherent propagation by which electrons reach the lobes proceeds at superluminal velocities of recession comparable to those observed in some quasars. Thus, focused transport gives rise to the radio source structures that are summarized in figure 12. Except for relatively slow changes which may occur in powerful sources due

to particle pressure, only static magnetic fields are involved. Consequently, the adiabatic energy losses that embarrass interpretations in which electrons are transported within expanding clouds of thermal plasma do not occur in the present model. Finally, the basic features of focused transport are confirmed by interplanetary observations. In retrospect, it seems surprising that the relationship between the scatter-free propagation of solar electrons and the intergalactic transport of radio emitting electrons had not been recognized.

This research was supported by the National Aeronautics and Space Administration under grant NGR-21-002-066. The extensive contributions of John W. Bieber are gratefully acknowledged.

## REFERENCES

- Abramowitz, M., and Stegun, I. A. 1964, N.B.S. Applied Mathematics Series, No. 55.
- Boukidis, N. A., and Ruggiero, R. J. 1949, Journal of Aeronautical Sciences, 11, 319.
- Branson, N. J. B. A., Ellsmore, B., Pooley, G. G., and Ryle, M. 1971, M.N.R.A.S., 156, 377.
- Bryant, D. A., Cline, T. L., Desai, U. D., and McDonald, F. B. 1965, Ap. J., 141, 478.
- Chenette, D. L., Conlon, T. F., and Simpson, J. A. 1974, J. Geophys. Res., 79, 3551.
- Cohen, M. H., Cannon, W., Purcell, G. H., Shaffer, D. B., Broderick, J. J., Kellerman, K. I., and Jauncey, D. L. 1971, Ap. J., 170, 207.
- Courant, R., and Hilbert, D. 1953, Methods of Mathematical Physics (New York: Interscience), Vol. 1.
- Earl, J. A. 1973, Ap. J., 180, 227 (Paper I).
- Earl, J. A. 1974a, Ap. J., 188, 379 (Paper II).
- Earl, J. A. 1974b, Ap. J., 193, 231 (Paper III).
- Evans, L. G., Fainberg, J., and Stone, R. G. 1973, Solar Phys., 31, 501.
- Fomalont, E. B. 1969, Ap. J., 157, 1027.
- Goldstein, M. L., Klimas, A. J., and Sandri, G. 1975, Ap. J., 195, 787
- Hargrave, P. J., and Ryle, M. 1969, M.N.R.A.S., 146, 221.
- Hildebrand, F. B. 1949, Advanced Calculus for Engineers (New York: Prentice Hall, Inc.).
- Jaffe, W. J., and Perola, G. C. 1973, Astr. and Ap., 26, 423.
- Jokipii, J. R. 1966, Ap. J., 146, 480.
- Jones, F. C., Kaiser, T. B., and Birmingham, T. J. 1973, Phys. Rev. Letters, 31, 485.

- Kundu, M. R. 1965, Solar Radio Astronomy (New York: Interscience).
- Lin, R. P. 1974, Space Sci. Rev., 16, 189.
- Lin, R. P., Evans, L. G., and Fainberg, J. 1973, Ap. Letters, 14, 191.
- Longair, M. S., Ryle, M., and Scheuer, P. A. G. 1973, M.N.R.A.S., 164, 243.
- McCracken, K. G. 1962, J. Geophys. Res., 67, 435.
- McCracken, K. G., Rao, U. R., and Bukata, R. P. 1967, J. Geophys. Res., 72, 4293.
- Macdonald, G. H., Kenderine, S., and Neville, A. C. 1968, M.N.R.A.S., 138, 259.
- Mackay, C. D. 1969, M.N.R.A.S., 145, 31.
- Mackay, C. D. 1971, M.N.R.A.S., 154, 209.
- Meyer, P., Parker, E. N., and Simpson, J. A. 1956, Phys. Rev., 104, 768.
- Miley, G. K. 1973, Astr. and Ap., 26, 413.
- Mitton, S. 1972, M.N.R.A.S., 155, 373.
- Nielsen, E., Pomerantz, M. A., and West, H. I. Jr. 1975, J. Geophys. Res.,  
80, XXXX.
- Owens, A. J. 1974, Ap. J., 191, 235.
- Pooley, G. G., and Henbest, S. N. 1974, M.N.R.A.S., 169, 477.
- Roelof, E. C. 1969, in Lectures in High Energy Astrophysics, ed. H.  
Ogelman and J. R. Wayland (Washington, D.C.: NASA SP-199).
- Ryle, M. 1975, Science, 188, 1071.
- Smith, E. J., Tsurutani, B. T., Chenette, D. L., Conlon, T. F., and Simpson,  
J. A. 1975, J. Geophys. Res., 80, XXXX.
- Teegarden, B. J., McDonald, F. B., Trainor, J. H., Webber, W. R., and Roelof,  
E. C. 1974, J. Geophys. Res., 79, 3615.
- Volk, H. J. 1973, Ap. and Space Sci., 25, 471.
- Wellington, K. J., Miley, G. K., and van der Laan, H. 1973, Nature 244, 502.
- Wentzel, D. G. 1974, Ann. Rev. Astr. and Ap., 12, 71.
- Whitney, A. R., Shapiro, I. I., Rogers, A. E. E., Robertson, D. S., Knight, C.A.,  
Clark, T. A., Goldstein, R. M., Marandino, G. E., and Vandenberg, N. R.  
1971, Science, 173, 225.

Willis, A. G., Strom, R. G., and Wilson, A. S. 1974, *Nature*, 250, 625.

JAMES A. EARL: Department of Physics and Astronomy, University of Maryland,  
College Park, Maryland 20742

## FIGURE CAPTIONS

Figure 1. The scattering eigenfunctions at the left, which were defined in Paper II, are symmetrical functions of  $\mu$ . In contrast, the focusing eigenfunctions at the right are asymmetrical.

Figure 2. The focusing eigenvalues increase monotonically with  $(V/AL)$ .

Figure 3. The four characteristic velocities that reduce in the absence of focusing to the finite velocities defined in Paper II all vanish when focusing becomes intense. This absence of coupling between eigenfunctions of opposite parity leads to supercoherent propagation.

Figure 4. For isotropic scattering,  $q = 1$ , the six characteristic velocities that vanish when focusing is absent display a complicated dependence upon  $(V/AL)$ . When the scattering is anisotropic, as it is at  $q = 1.5$  and  $q = 1.9$ , this intricate pattern is dramatically simplified.

Figure 5. This graph shows that the artificial decay associated with the truncated set of equations that describe focused diffusion plays an unimportant role in the overall evolution of the distribution function.

Figure 6. The coherent velocities,  $V_+$  and  $V_-$ , that appear in focused diffusion are not strongly dependent on  $(V/AL)$ .

Figure 7. This graph shows that  $\kappa_2 \approx (1/2L)$ .

Figure 8. Density profiles which compare ordinary diffusion (a) to focused diffusion with positive injection velocity (b) and to focused diffusion with negative injection velocity (c).

Figure 9. The velocities that describe the supercoherent mode are plotted as functions of  $(V/AL)$ .

Figure 10. A supercoherent density profile is compared to the corresponding profile for focused diffusion.

Figure 11. Schematic diagram of the solar neighborhood showing three regions in which there appear qualitatively different solar event profiles.

Figure 12. An atlas of radio source configurations that can be explained in terms of ideas presented in this paper: (a) two symmetrical lobes of emission on opposite sides of the central galaxy, (b) two secondary lobes between the primary lobes, (c) a succession of lobes deployed behind a moving galaxy, and (d) two compact lobes moving away from the central galaxy with velocities slightly less than that of light.

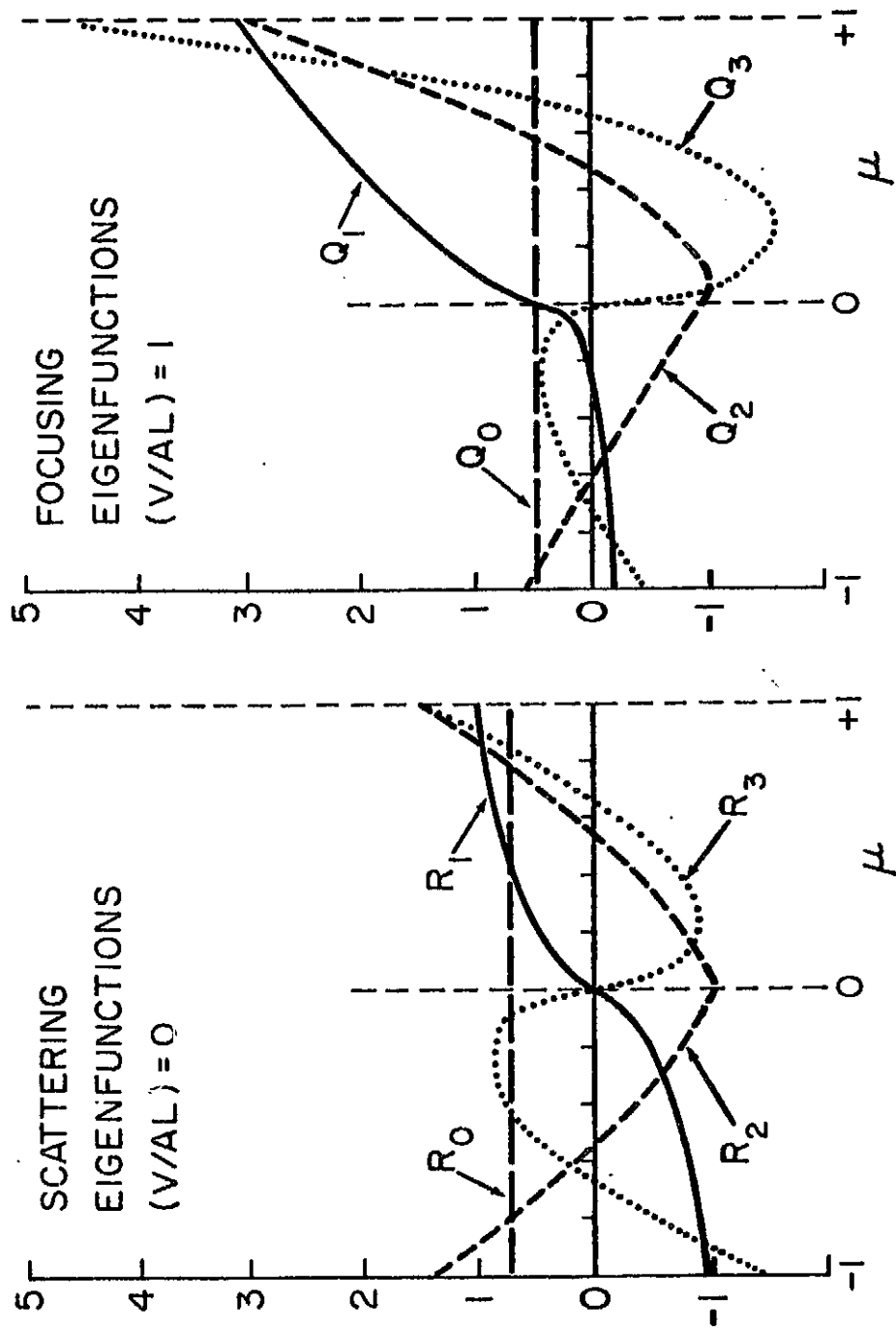


FIGURE 1

PRECEDING PAGE BLANK NOT FILMED

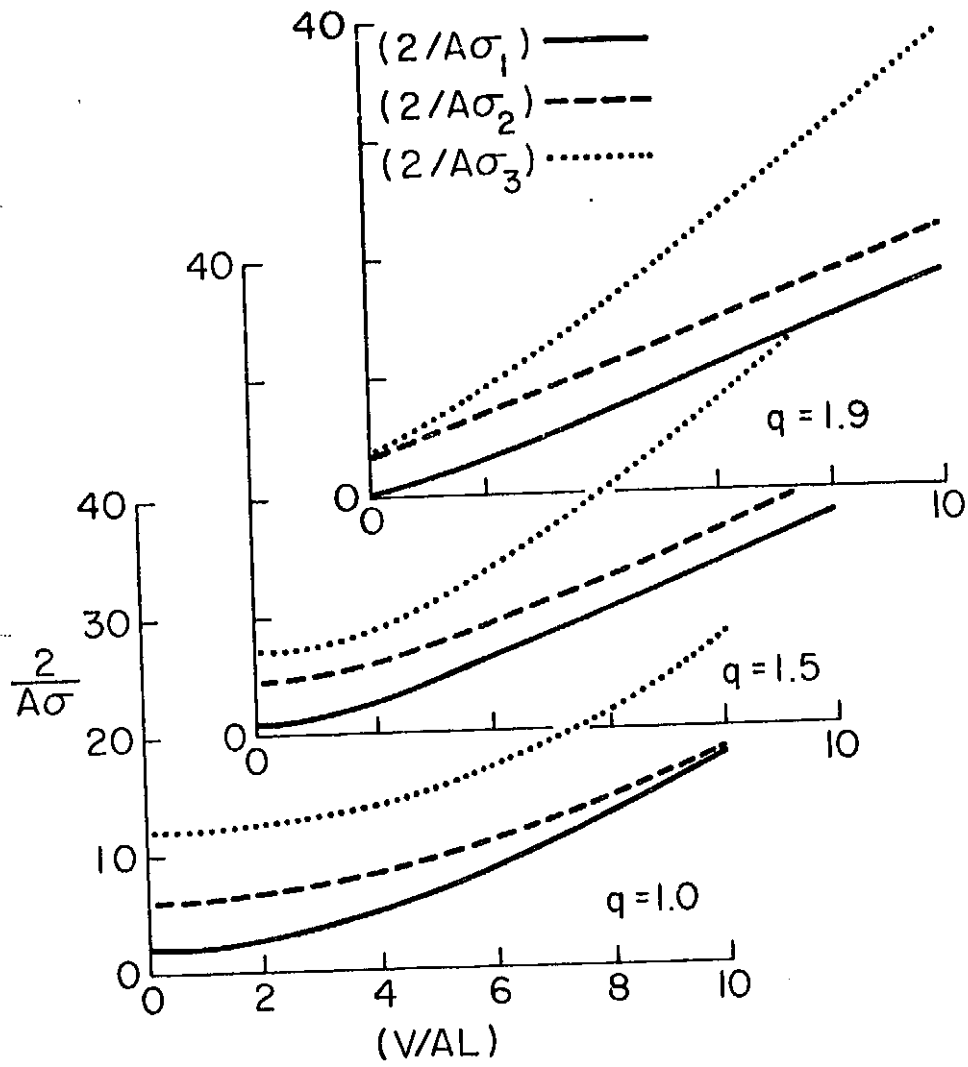


FIGURE 2

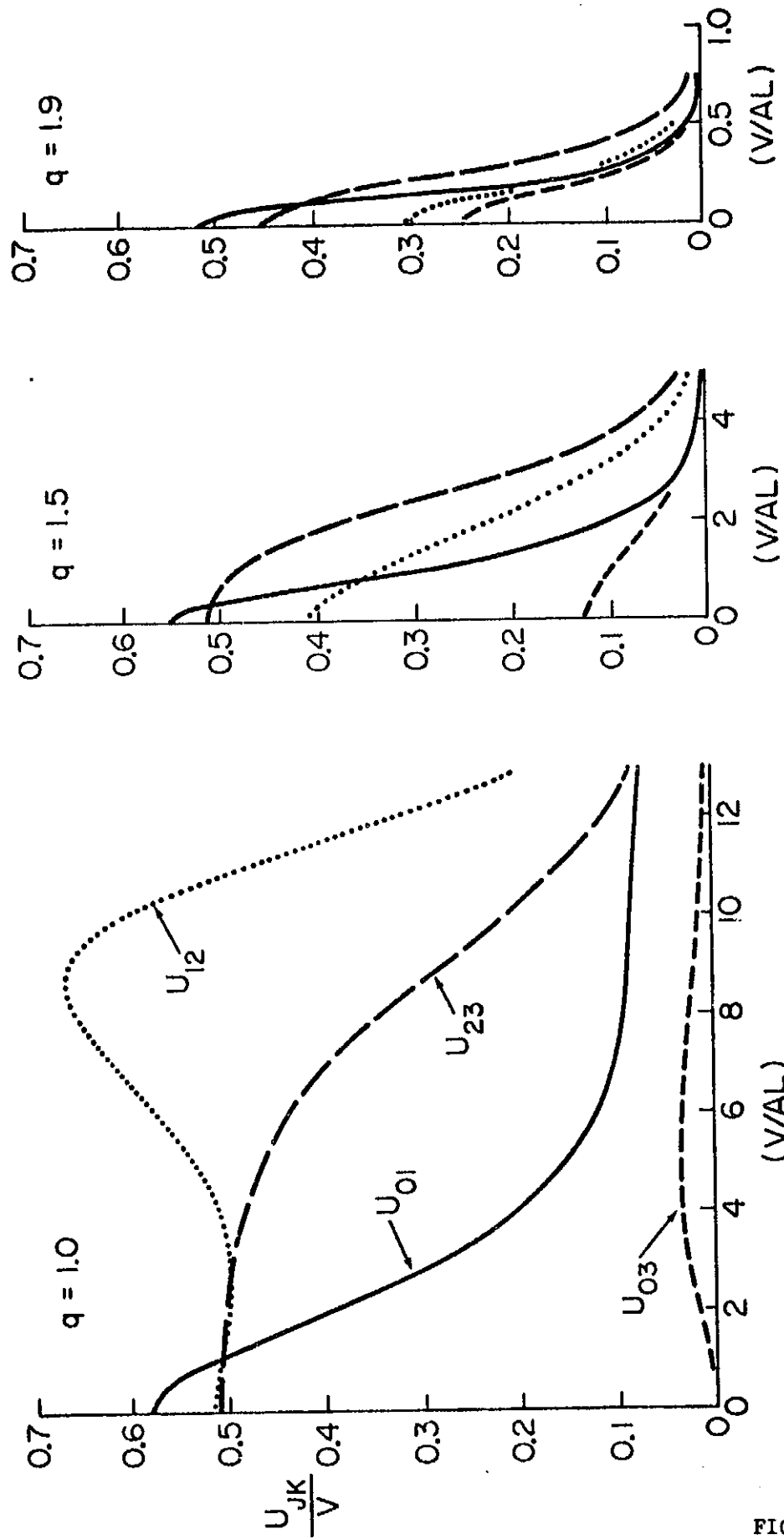


FIGURE 3

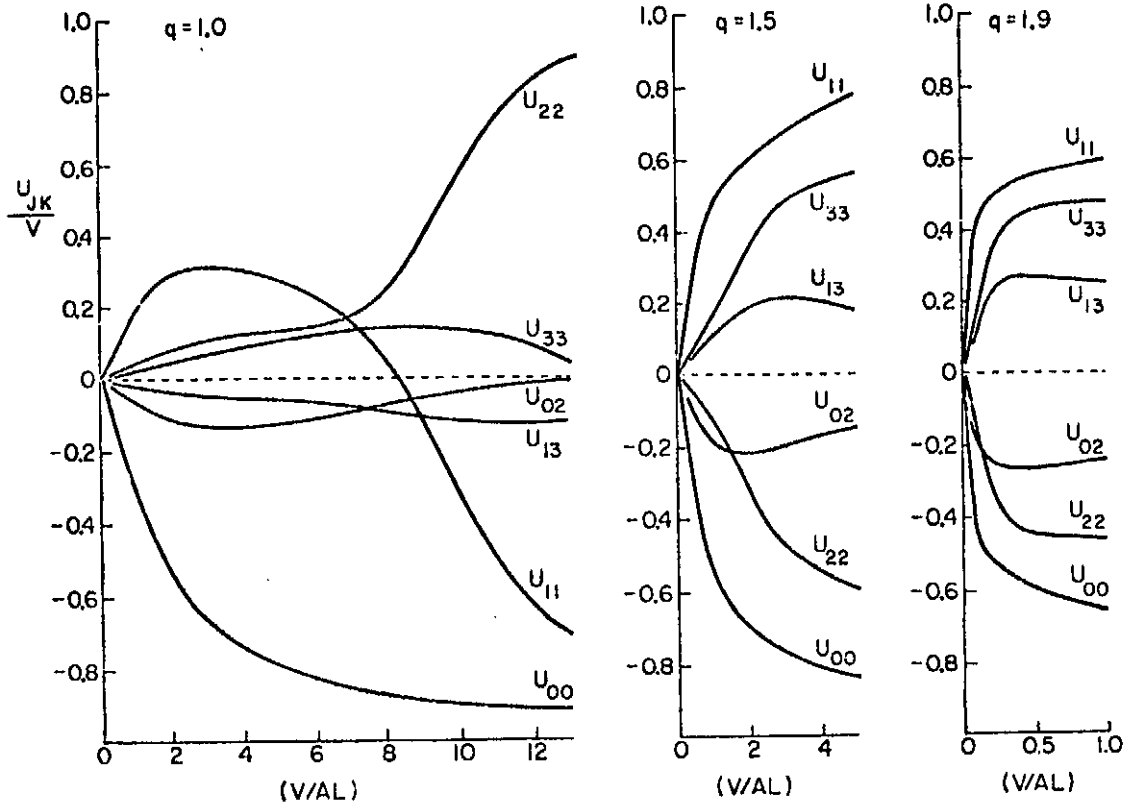


FIGURE 4

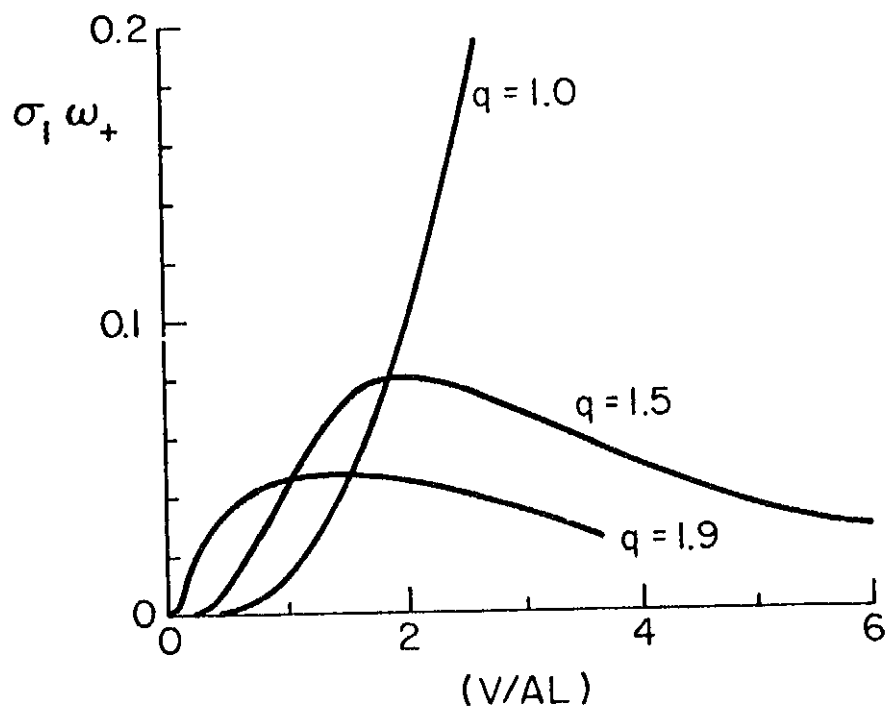


FIGURE 5

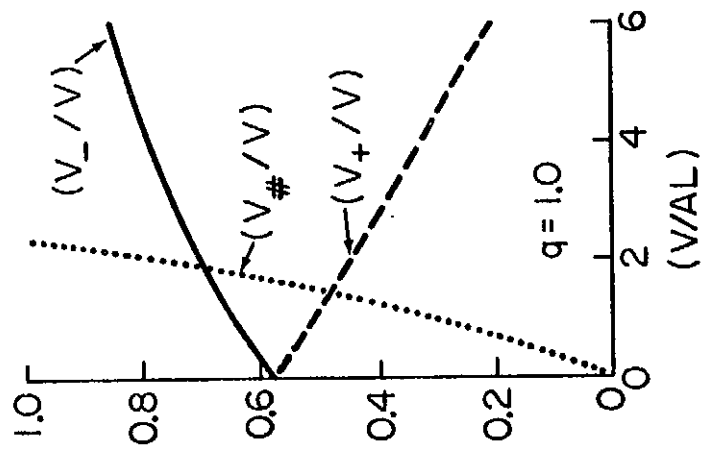
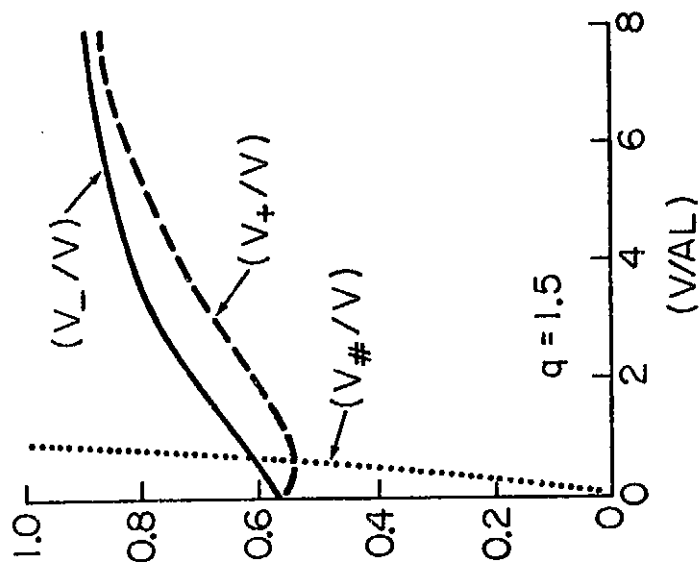
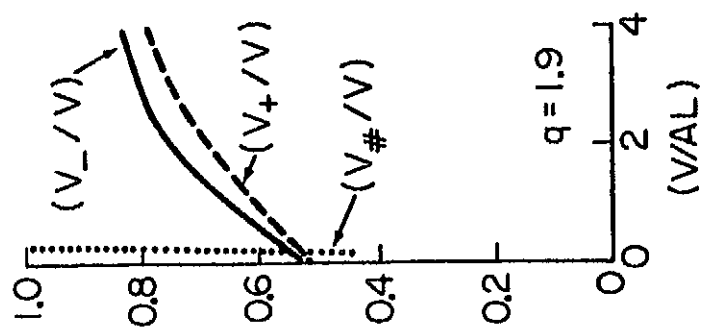


FIGURE 6

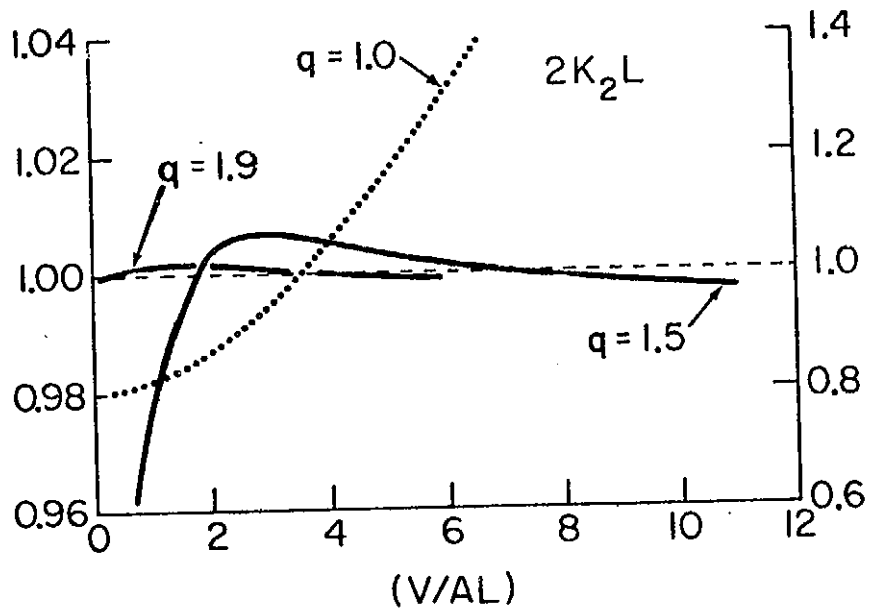


FIGURE 7

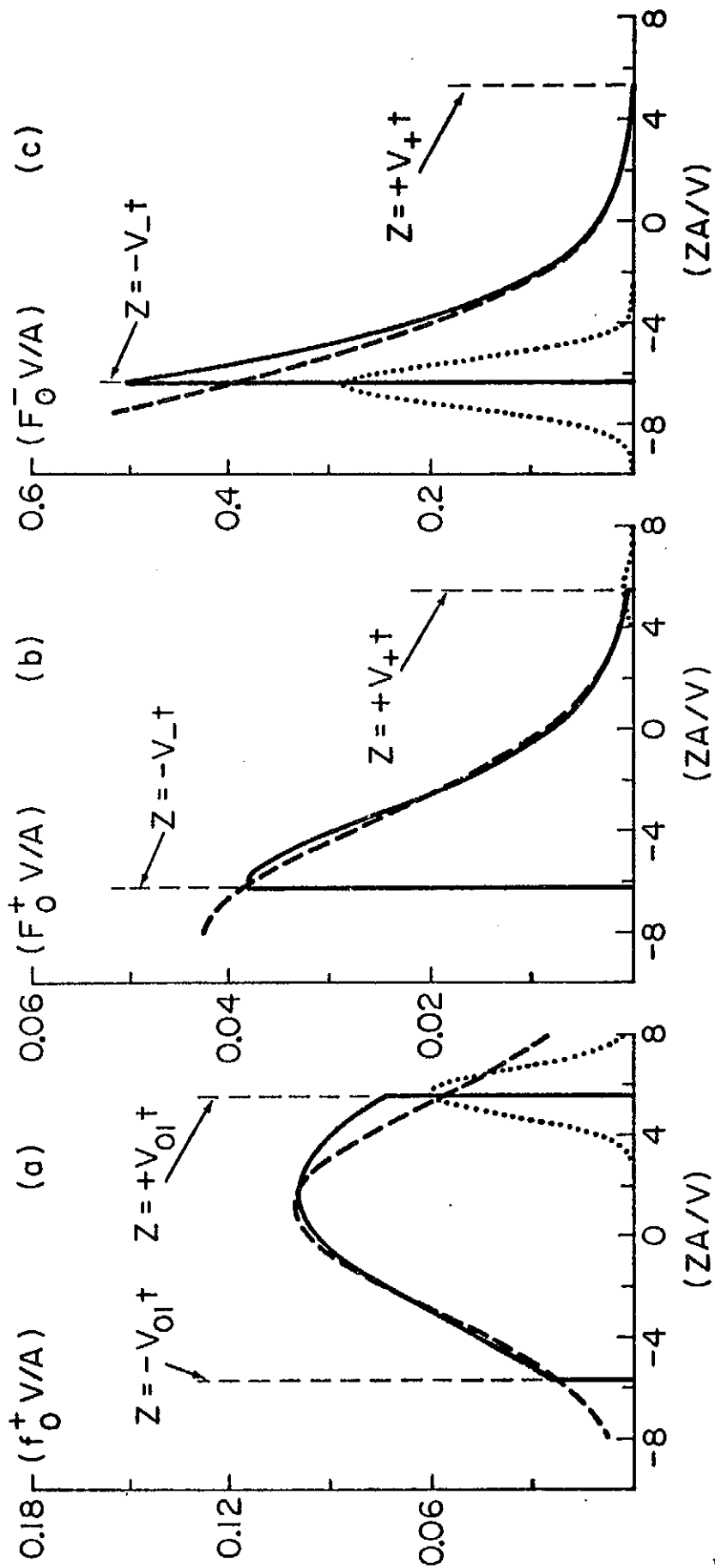


FIGURE 8

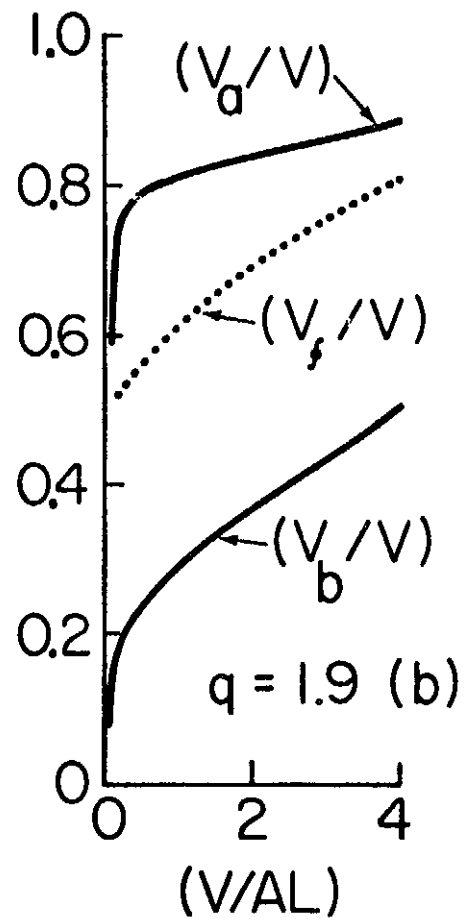
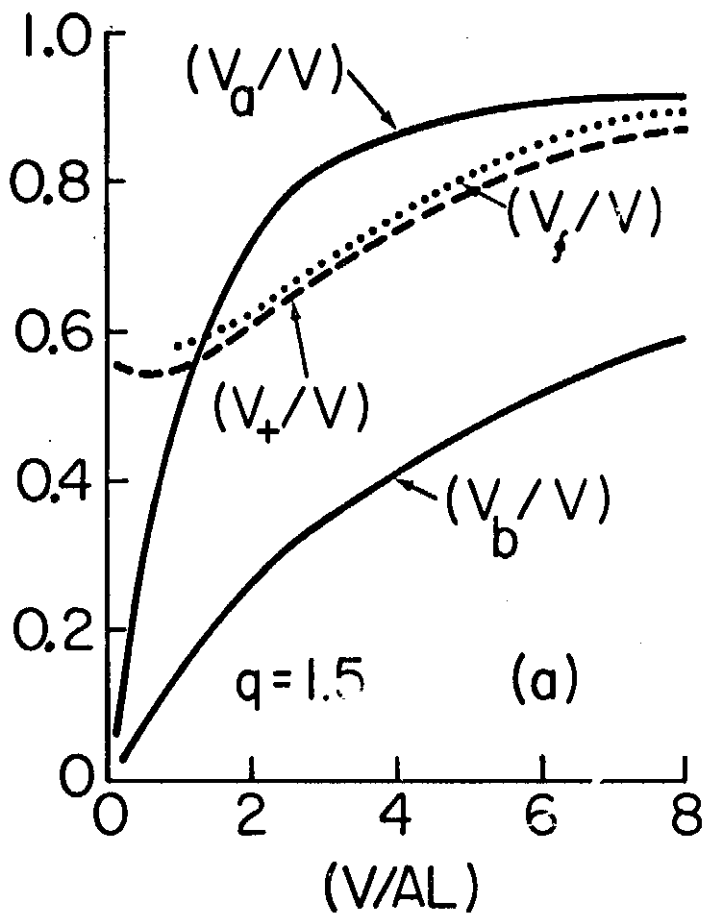
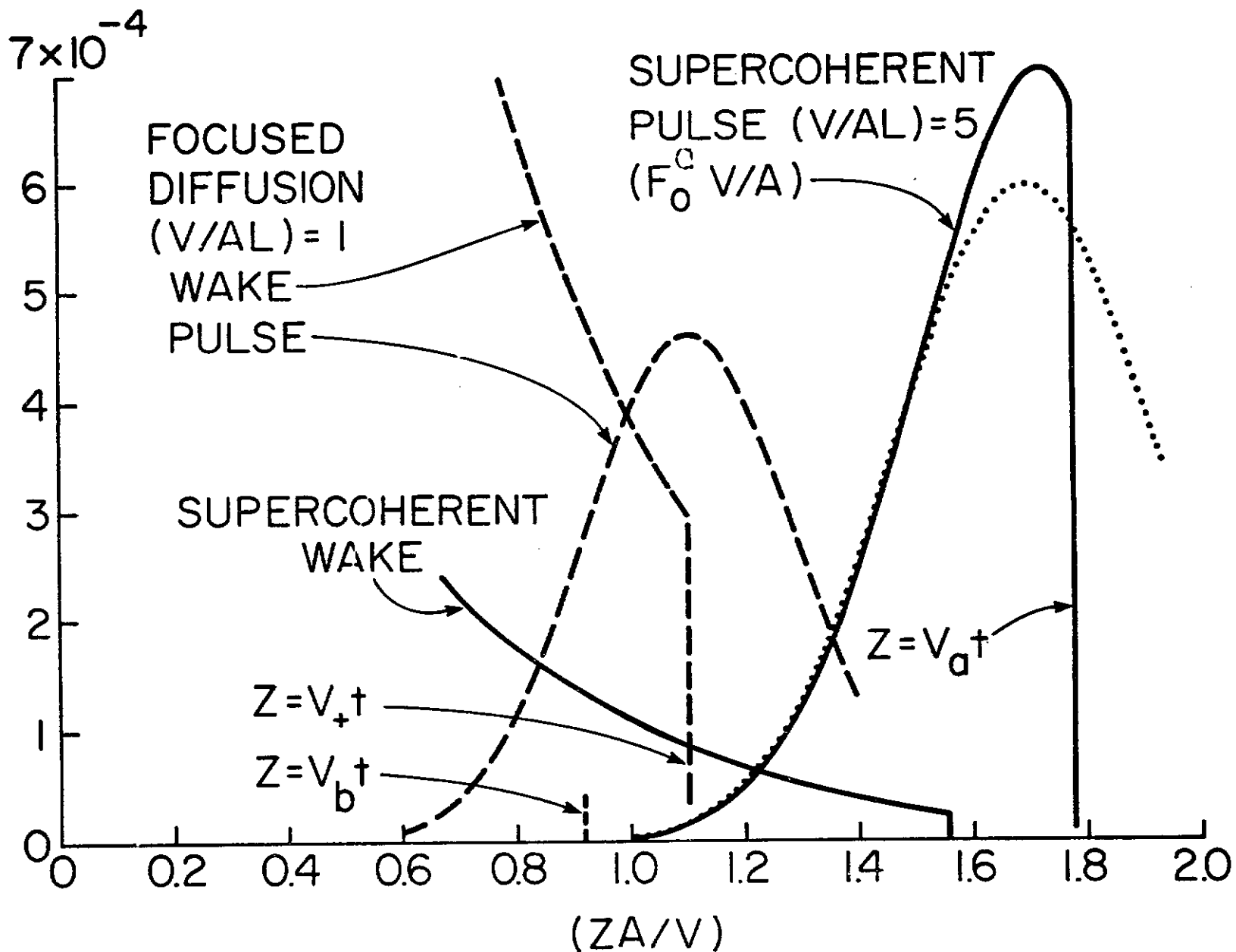


FIGURE 9

FIGURE 10



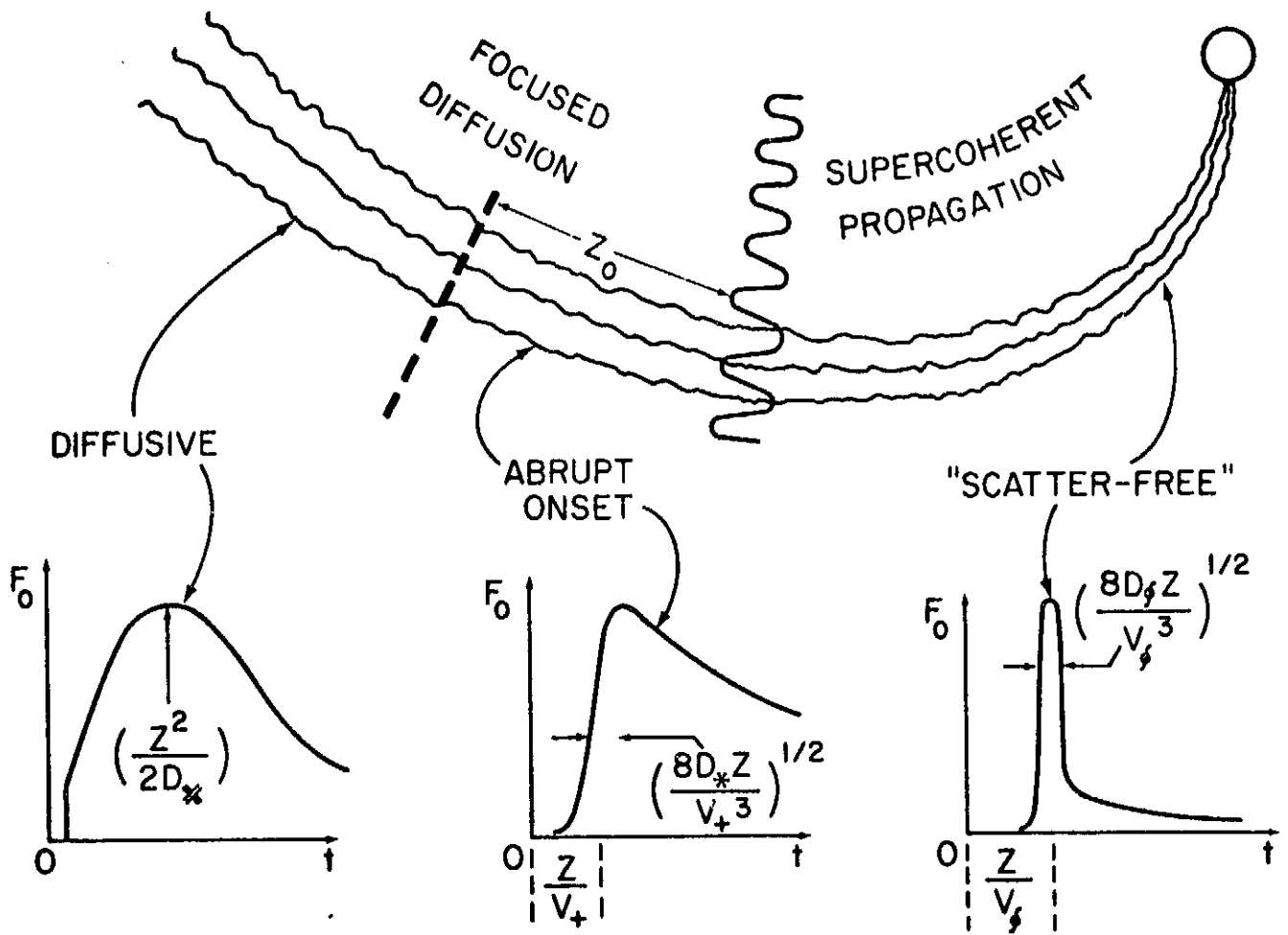


FIGURE 11

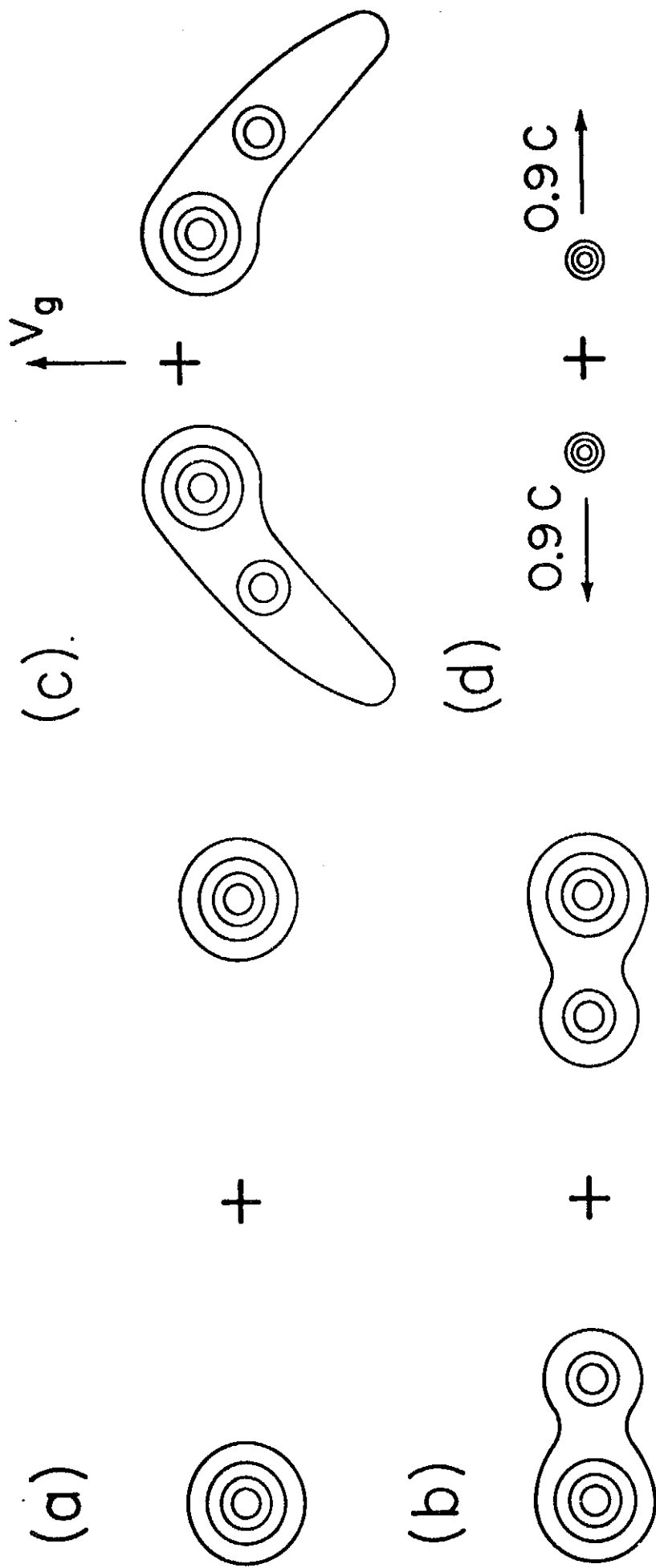


FIGURE 12

ORIGINAL PAGE IS  
OF POOR QUALITY

TABLE I

FOCUSING EIGENVALUES AND CHARACTERISTIC VELOCITIES

$\rho$	$\frac{v}{AL}$	$\frac{2}{A\sigma_1}$	$\frac{2}{A\sigma_2}$	$\frac{2}{A\sigma_3}$	$\frac{U_{00}}{V}$	$\frac{U_{01}}{V}$	$\frac{U_{02}}{V}$	$\frac{U_{03}}{V}$	$\frac{U_{11}}{V}$	$\frac{U_{12}}{V}$	$\frac{U_{13}}{V}$	$\frac{U_{22}}{V}$	$\frac{U_{23}}{V}$	$\frac{U_{33}}{V}$
1.0	0.0	2.00	6.03	12.01	.0000	.5783	.0000	.0000	.0000	.5153	.0000	.0000	.5090	.0000
	1.0	2.20	6.17	12.14	-.3139	.5211	-.0696	.0046	.1836	.5094	-.0202	.0439	.5075	.0238
	2.0	2.80	6.59	12.55	-.5383	.4006	-.1143	.0150	.2866	.4993	-.0358	.0810	.5031	.0467
	3.0	3.79	7.29	13.22	-.6723	.2879	-.1314	.0252	.3137	.4967	-.0461	.1073	.4956	.0675
	4.0	5.13	8.24	14.19	-.7510	.2070	-.1304	.0320	.3012	.5068	-.0531	.1226	.4843	.0856
	5.0	6.81	9.43	15.46	-.8003	.1545	-.1207	.0344	.2712	.5303	-.0588	.1307	.4671	.1013
	6.0	8.76	10.83	17.06	-.8134	.1221	-.1077	.0331	.2283	.5665	-.0658	.1406	.4403	.1147
	7.0	10.89	12.41	19.06	-.8572	.1034	-.0935	.0291	.1632	.6118	-.0766	.1684	.4000	.1259
	8.0	13.12	14.13	21.51	-.8750	.0939	-.0784	.0236	.0559	.6541	-.0922	.2381	.3449	.1339
	9.0	15.36	15.94	24.45	-.8889	.0899	-.0620	.0180	-.1110	.6645	-.1101	.3707	.2794	.1368
10.0	17.56	17.83	27.89	-.9000	.0880	-.0447	.0134	-.3212	.6046	-.1242	.5517	.2129	.1323	
1.5	0.0	.80	4.42	7.05	.0000	.5626	.0000	.1278	.0000	.4109	.0000	.0000	.5120	.0000
	0.5	.93	4.53	7.14	-.3556	.4630	-.1181	.1192	.3087	.3867	.0591	-.0588	.5059	.0830
	1.0	1.32	4.84	7.43	-.5544	.2916	-.1863	.1007	.4721	.3367	.1088	-.1308	.4855	.1698
	1.5	1.92	5.34	7.92	-.6483	.1660	-.2115	.0795	.5480	.2819	.1520	-.2234	.4434	.2636
	2.0	2.66	5.99	8.64	-.7012	.0911	-.2139	.0579	.5983	.2235	.1877	-.3258	.3738	.3563
	2.5	3.49	6.72	9.59	-.7377	.0489	-.2058	.0381	.6411	.1637	.2103	-.4157	.2841	.4324
	3.0	4.37	7.51	10.76	-.7659	.0257	-.1933	.0229	.6785	.1105	.2178	-.4793	.1952	.4832
	3.5	5.28	8.33	12.09	-.7889	.0132	-.1799	.0129	.7105	.0700	.2142	-.5203	.1244	.5137
	4.0	6.21	9.17	13.54	-.8080	.0067	-.1671	.0070	.7380	.0424	.2049	-.5487	.0754	.5334
	4.5	7.16	10.03	15.08	-.8240	.0034	-.1555	.0037	.7616	.0249	.1934	-.5715	.0442	.5487
5.0	8.13	10.92	16.68	-.8378	.0017	-.1451	.0020	.7823	.0144	.1815	-.5919	.0253	.5626	
1.9	0.00	.11	3.21	3.66	.0000	.5178	.0000	.2549	.0000	.3115	.0000	.0000	.4559	.0000
	0.25	.28	3.52	3.85	-.5393	.3094	-.2573	.0944	.5170	.1230	.2542	-.3724	.2556	.3847
	0.50	.57	3.93	4.40	-.5915	.0119	-.2644	.0158	.5538	.0224	.2703	-.4479	.0548	.4670
	0.75	.91	4.33	5.04	-.6271	.0013	-.2525	.0020	.5789	.0031	.2629	-.4560	.0080	.4777
	1.00	1.26	4.74	5.70	-.6573	.0001	-.2403	.0002	.6024	.0004	.2547	-.4639	.0010	.4852
	1.25	1.64	5.17	6.40	-.6832	-	-.2288	-	.6244	-	.2465	-.4735	.0001	.4927
	1.50	2.03	5.61	7.11	-.7057	-	-.2179	-	.6450	-	.2384	-.4844	-	.5002
	1.75	2.44	6.06	7.85	-.7253	-	-.2078	-	.6641	-	.2304	-.4959	-	.5077
	2.00	2.85	6.51	8.60	-.7425	-	-.1984	-	.6819	-	.2226	-.5078	-	.5151
	2.25	3.28	6.98	9.38	-.7577	-	-.1897	-	.6984	-	.2150	-.5199	-	.5226
2.50	3.72	7.45	10.17	-.7713	-	-.1817	-	.7136	-	.2075	-.5318	-	.5299	

ENCLOSING PAGE BLANK NOT FILMED